Chem. Eur. J. **2003**

Supporting Information

for

Towards Binuclear Polyaminocarboxylate MRI Contrast Agents? Spectroscopic and MD Study of the Peculiar Aqueous Behaviour of $Ln_2(OHEC)^{2-}$ (Ln = Eu, Gd and Tb) : Implications for Relaxivity.

By

Gaëlle M. Nicolle,[a] Fabrice Yerly,[a] Daniel Imbert,[b] Ulrike Böttger,[c] Jean- Claude Bünzli [b] and André E. Merbach[a]

Figure S1. 400 MHz ^{1}H COSY45 spectrum of $Eu_2(OHEC)^{2-}$ at 273.6 K.

Figure S2. 600 MHz ^{1}H Clean-TOCSY spectrum of $Eu_2(OHEC)^{2-}$ at 273.6 K.

Figure S3. 400 MHz ^{13}C HMQC spectrum of $Eu_2(OHEC)^{2-}$ at 268.2 K.

Figure S4. 600 MHz ^{1}H NOESY spectrum of $Eu_2(OHEC)^{2-}$ at 274.8 K, t_m = 60 ms.

Figure S5. pH dependence of 600 MHz ^{1}H NMR spectra of $Eu_2(OHEC)^{2-}$.

Figure S6. Temperature dependence of 600 MHz ^{1}H NMR spectra of $Eu_2(OHEC)^{2-}$.

Figure S7. Pressure dependence of 400 MHz ^{1}H NMR spectra of $Eu_2(OHEC)^{2-}$.

Figure S8. Temperature dependence of 400 MHz ^{1}H NMR spectra of $Tb_2(OHEC)^{2-}$.

Figure S9. one dimensional representation of the temperature dependence of the $^{7}F_0$-$^{5}D_0$ transition on the UV-vis spectra of $Eu_2(OHEC)^{2-}$. C_{Eu} ~ 30 mmol kg^{-1}.

Figure S10. one dimensional representation of the pressure dependence of the $^{7}F_0$-$^{5}D_0$ transition on the UV-vis spectra of $Eu_2(OHEC)^{2-}$. C_{Eu} ~ 10 mmol kg^{-1}.

Equation S1. Equations used for the simultaneous fit of variable temperature EPR spectra.

Equation S2. Equations used for the simultaneous fit of variable temperature and pressure UV-vis spectra.

Equation S3. Equations used for the simultaneous fit of variable temperature ^{17}O NMR EPR and ^{1}H NMRD data.

Figure S11. Temperature dependence of EPR spectra of the $Gd_2(OHEC)^{2-}$ and its *a* and *b* isomers at X-band. The dotted lines represent the calculated spectra calculated for each isomer.

Figure S12. Temperature dependence of EPR spectra of the $GdY(OHEC)^{2-}$ and its *a* and *b* isomers at X-band. The dotted lines represent the calculated spectra calculated for each isomer.

Figure S13. pH dependence of the relaxivity of $Gd_2(OHEC)^{2-}$.

Figure S14. Pressure dependence of the increase of the ^{17}O transverse relaxation rate ($1/T_{2P}$) at 312 K and 9.4 T due to $[Gd_2(OHEC)(H_2O)_2]^{2-}$. C_{Gd} = 45.17 mmol kg^{-1}.

Figure S15. Emission spectra of the $Eu_2(OHEC).H_2O$ complex in solid state at 295 K, upon broad ($^5D_2$) band and selective excitation.

Figure S16. Excitation spectra at 295 K of the $Eu_2(OHEC).H_2O$ complex in solid state, upon monitoring the Eu($^5D_0 \rightarrow {}^7F_{1,\ 2}$) transitions and enlargement (top) of the Eu($^5D_0 \rightarrow {}^7F_0$) transition (broad band excitation($^5D_2$)).

Figure S17. Emission spectra of the $Eu_2(OHEC).H_2O$ complex in solution (10^{-3} M), at 295 K, upon broad band ($^5D_2$) and selective excitation.

Figure S18. Emission spectra of the $Eu_2(OHEC).H_2O$ complex in solution (10^{-4} M), at 295 K, upon broad band and selective excitation.

Figure S19. Normalised emission spectra of the $Eu_2(OHEC).H_2O$ complex in solution (10^{-3} M), at 295 K, upon broad band and selective excitation.

Figure S20. Time evolution of the α and β isomers dihedral angles during the MD-*a* and MD-*b* simulations. The radial part represents the time in picosecond while the azimutal angle angle represents the dihedral angles.

Figure S21. Angular projections of the Gd^{III} coordination polyhedrons centred on the C_4 axis. Upper part : projection of the two coordination polyhedrons in MD-*a*. Lower part : corresponding projections in MD-*b*.

Table S1. Ratio of the molar fraction of the 2 isomers *a* and *b* of $Eu_2(OHEC)^{2-}$, $x_b/x_a = K$, obtained from the 600MHz ^1H NMR study at variable temperature.

Table S2. Ratio of the molar fraction of the 2 isomers *a* and *b* of $Eu_2(OHEC)^{2-}$, $x_b/x_a = K$, obtained from the variable pressure study at 400MHz and, at 279.4 K.

Table S3. Half line widths ($1/T_2$) of the protons ^{2}E', ^{2}e' (×2) from the experimental 600 MHz ^{1}H NMR spectra of $Eu_2(OHEC)^{2-}$ measured at variable temperature.

Table S4. Extrapolated half line widths ($1/T_2$) of the protons ^{2}E', ^{2}e' (×2) from the experimental 600 MHz ^{1}H NMR spectra of $Eu_2(OHEC)^{2-}$ measured at variable temperature.

Table S5. Isomerisation constant, k_{is}, obtained from the simulation of the experimental 600 MHz ^{1}H NMR spectra of $Eu_2(OHEC)^{2-}$ measured at variable temperature with the formalism of Kubo-Sack and a 3 sites exchange matrix (protons: ^{2}E', ^{2}e' (×2)).

Table S6. Half line widths ($1/T_2$) of the protons ^{2}E', ^{2}e' (×2) from the experimental 400 MHz ^{1}H NMR spectra of $Eu_2(OHEC)^{2-}$ measured at variable pressure and at 279.4 K.

Table S7. Extrapolated half line widths of the experimental 400 MHz ^{1}H NMR spectra of $Eu_2(OHEC)^{2-}$ measured at variable pressure and at 279.4 K.

Table S8. Kinetics constant, k_{is}, obtained from the simulation of the experimental 400 MHz ^{1}H NMR spectra of $Eu_2(OHEC)^{2-}$ measured at variable pressure with the formalism of Kubo-Sack and a 3 sites exchange matrix (protons: ^{2}E', ^{2}e' (×2)).

Table S9. ^{17}O observed longitudinal and transverse relaxation rates at 9.4 T as a function of temperature for the diamagnetic reference at pH = 9 ($1/T_{1A}$ and $1/T_{2A}$) and in the presence of $Gd_2(OHEC)^{2-}$ ($1/T_1$ and $1/T_2$). Solutions of $Gd_2(OHEC)^{2-}$: C_{Gd} = 21.87 mmol kg^{-1}.

Table S10. ^{17}O chemical shift of the diamagnetic reference, δ_A, and in the presence of $Gd_2(OHEC)^{2-}$, δ, at 9.4 T as a function of temperature. Solutions of $Gd_2(OHEC)^{2-}$: C_{Gd} = 21.87 mmol kg^{-1}.

Table S11. Pressure dependence of the increase of the ^{17}O transverse relaxation rate ($1/T_{2P} = 1/T_{2,obs} - 1/T_{2A}$) due to $[Gd_2(OHEC)(H_2O)_2]^{2-}$ and of the diamagnetic reference ($1/T_{2A}$) (bidistilled water at pH =9) at 312 K and 9.4 T. C_{Gd} = 45.17 mmol kg^{-1}.

Table S12. ^{17}O transverse relaxation rates at 4.7 T as a function of temperature for the diamagnetic reference at pH = 9 ($1/T_{2A}$) and in the presence of $Gd_2(OHEC)^{2-}$ ($1/T_2$). Solutions of $Gd_2(OHEC)^{2-}$: C_{Gd} = 21.87 mmol kg^{-1}.

Table S13. Half line widths (W) and centres (C) of the bands of α and β isomers measured at variable temperature by UV-vis. The obtained equilibrium constant K is given for each temperature. C_{Eu} ~ 30 mmol kg^{-1}.

Table S14. Half line widths (W) and centres (C) of the bands of α and β isomers measured at variable pressure by UV-vis. The obtained equilibrium constant K is given for each temperature. C_{Eu} ~ 10 mmol kg^{-1}.

Table S15. Peak to peak line widths and resonance frequency of the EPR spectra of $Gd_2(OHEC)^{2-}$, for its two *a* and *b* isomers, and the equilibrium constant K, as a function of temperature at the X-band (0.34 T). Solutions of $Gd_2(OHEC)^{2-}$: C_{Gd} = 40.7 mmol kg^{-1}.

Table S16. Water proton relaxivity, r_1 (in mM^{-1}s^{-1}) of $Gd_2(OHEC)^{2-}$ as a function of temperature and magnetic field. Solution of $Gd_2(OHEC)^{2-}$, C^a_{Gd} = 1.88 mmol dm^{-3}.

Table S17. Peak to peak line widths and resonance frequency of the EPR spectra of $GdY(OHEC)^{2-}$ for its two *a* and *b* isomers, and the equilibrium constant K, as a function of temperature at the X-band (0.34 T). Solutions of $GdY(OHEC)^{2-}$: C_{Gd} = 5.3 mmol kg^{-1}.

Table S18. Integrated and corrected relative intensities of the Eu($^5D_0 \rightarrow {}^7F_j$) transitions at 295 K.

Table S19. Energy (cm^{-1}) of the identified crystal-field sub-levels of the Eu(^7F_j) manifold (J = 1-4) in $Eu_2(OHEC).H_2O$ as determined from excitation and emission spectra in solid state or in water solution at 295 K; $^7F_0$ is taken as the origin.

Table S20. Lifetimes of the Eu($^5D_0$) excited level (ms) in the Eu_2(OHEC).H_2O complex under various excitation conditions (analysing wavelength set on the maximum of the $^5D_0 \rightarrow {}^7F_2$);2 σ is given within parentheses.

Table S21. Calculated number of water molecules *q*.

Table S22. Selected time averaged dihedral angles calculated from MD simulations. Numbers in brackets are one standard deviation.

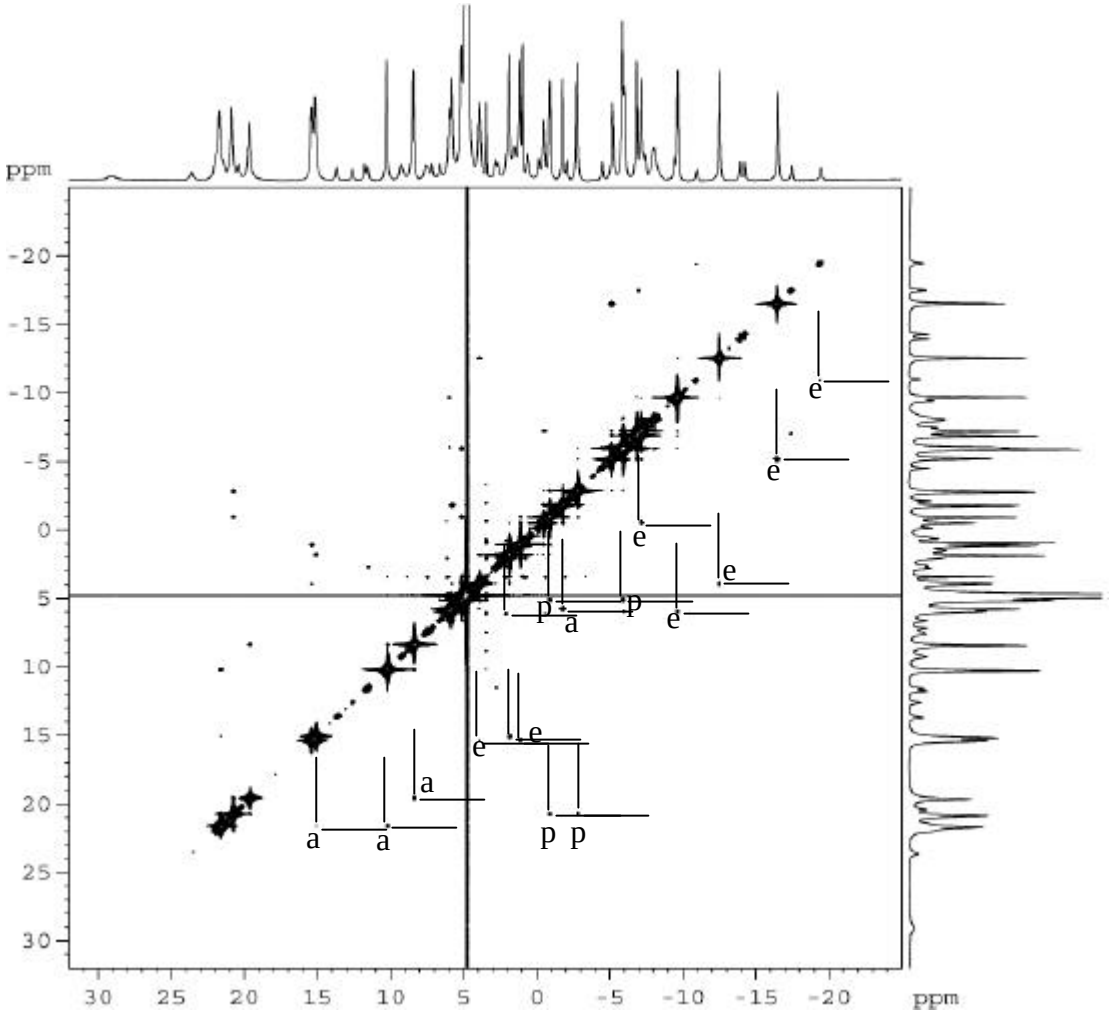

Figure S1. 400 MHz ^{1}H COSY45 spectrum of $Eu_2(OHEC)^{2-}$ at 273.6 K.

The 400MHz ^{1}H-COSY45 spectrum was recorded at 273.6 K with 56 scans with 1024 increments of 2048 data points and the same values for the zero-filled data points. The assignment of the nature of the protons (propylene = p, ethylene = e and acetate = a) for the major isomer has been established in agreement with the ^{1}H clean-TOCSY spectrum. According to the COSY spectrum there are couplings between (1P'', 3P'') (3P', 3P'') (1P'', 2P'') and (2P'', 2P'). The TOCSY confirmed the attribution of the propylene protons thanks to the cross-peak (1P'', 2P'). The rest of the crosspeaks on the TOCSY spectrum can be mainly accounted for the ethylene protons.

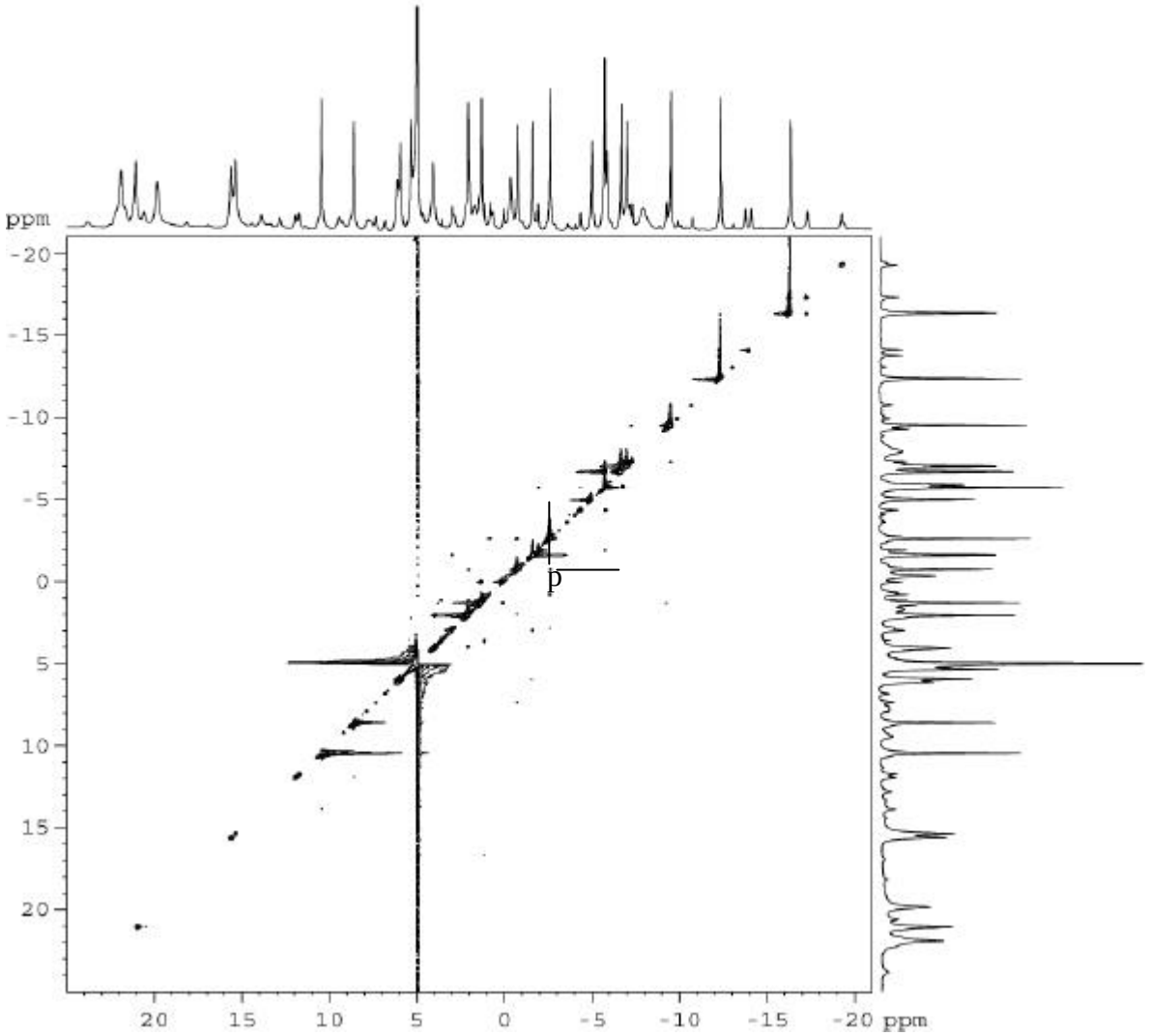

Figure S2. 600 MHz ^{1}H Clean-TOCSY spectrum of $Eu_2(OHEC)^{2-}$ at 273.6 K.

The 600 MHz ^{1}H Clean-TOCSY spectrum was recorded with a MLEV 17 sequence with trim-pulses after 16 scans at 273.6 K. The spin lock time was 12 ms. The number of data points were 4096 $t_2 \times 1600$ t_1 data points for the acquisition and 2048 $t_2 \times 2048$ t_1 data points for the zero-filled.

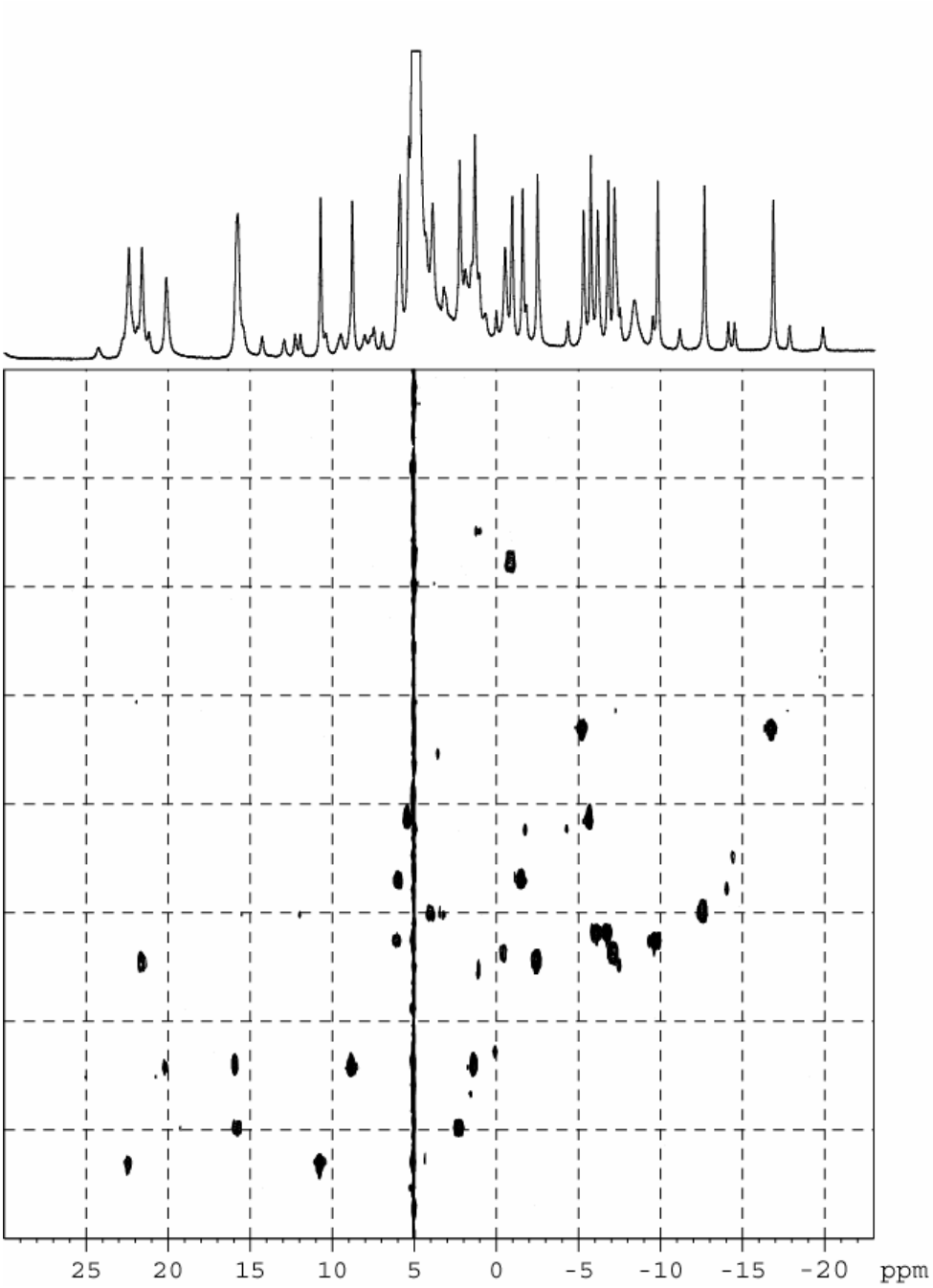

Figure S3. 400 MHz ^{13}C HMQC spectrum of $Eu_2(OHEC)^{2-}$ at 268.2 K.

400 MHz natural abundance ^{1}H-^{13}C HMQC spectrum was recorded at 268.2 K with a BIRD pulse sequence for the preparation period and decoupled during the acquisition and then treated with time proportional phase incrementation (TPPI). The optimised delay for inversion recovery of the magnetisation, τ, was 265 ms. 6144 $t_2 \times 512$ t_1 data points and 8192 $t_2 \times 1024$ t_1 data points for the zero-filled were used to obtain the spectrum, which consisted of 56 scans.

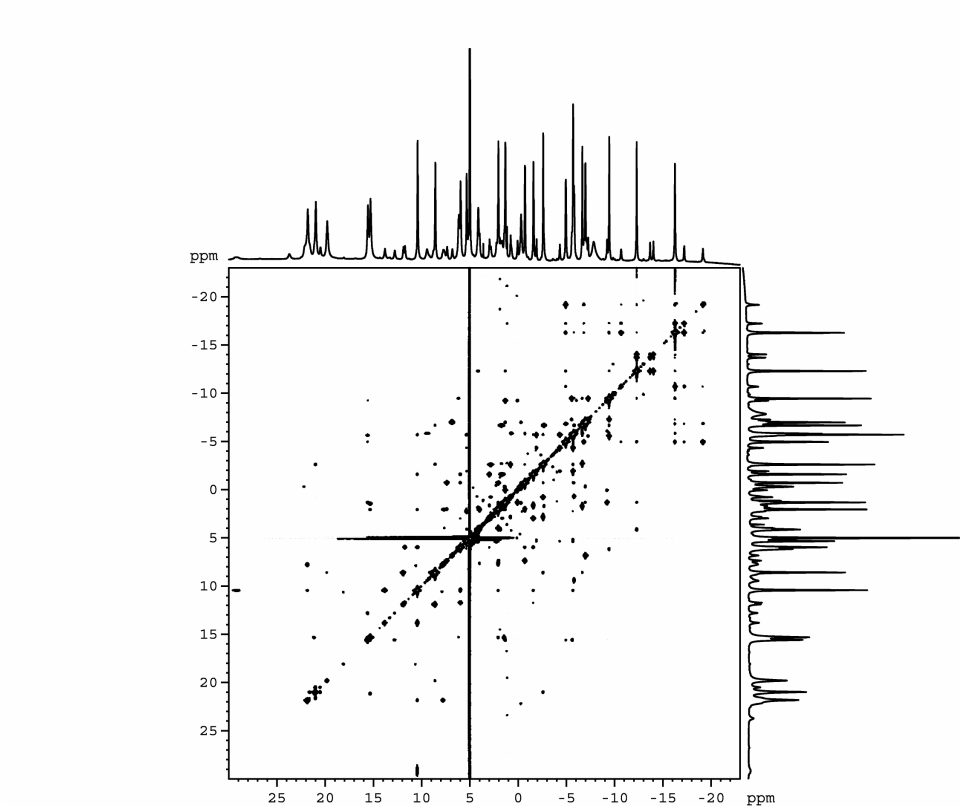

Figure S4. 600 MHz ^{1}H NOESY spectrum of $Eu_2(OHEC)^{2-}$ at 274.8 K, t_m = 60 ms.

A 600 MHz spectrum was recorded at 274.8 K using the conventional NOESY phase sensitive pulse sequence (90°-t_1-90°- τ_m-90°-acq) with 8192 $t_2 \times 1024$ t_1 data points and apodized with TPPI and zero filled to 8192 $t_2 \times 2048$ t_1. The number of scans was 100 and the mixing time, τ_m, equal to 60 ms.

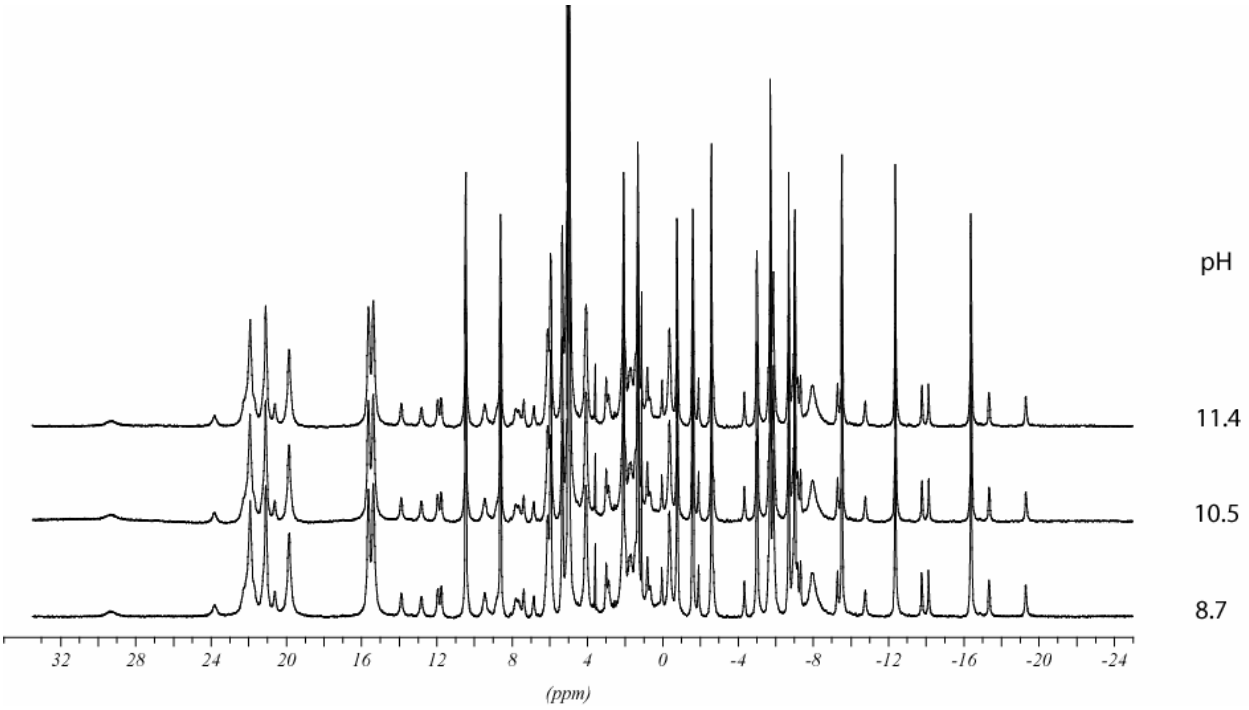

Figure S5. pH dependence of 600 MHz ^{1}H NMR spectra of $Eu_2(OHEC)^{2-}$ at 274.8 K.

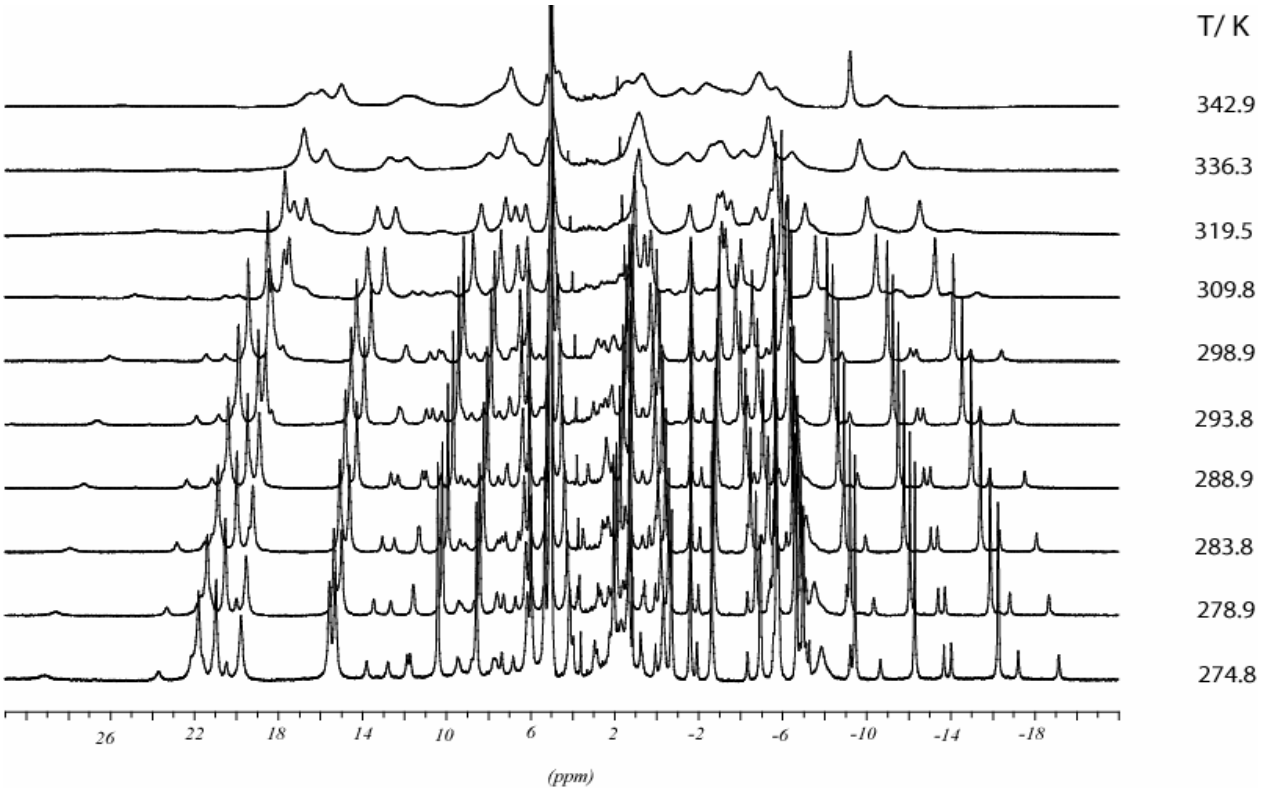

Figure S6. Temperature dependence of 600 MHz ^{1}H NMR spectra of $Eu_2(OHEC)^{2-}$.

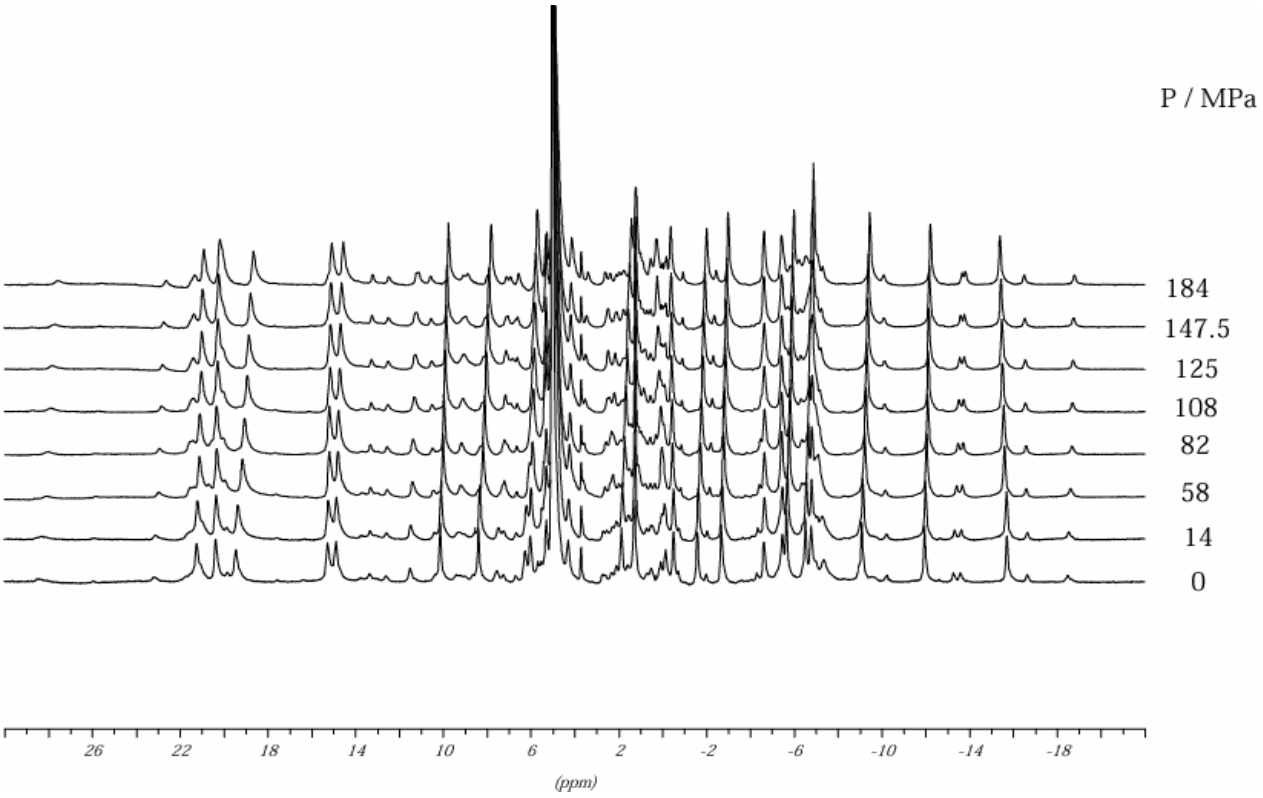

Figure S7. Pressure dependence of 400 MHz ^{1}H NMR spectra of $Eu_2(OHEC)^{2-}$ at 279.4 K.

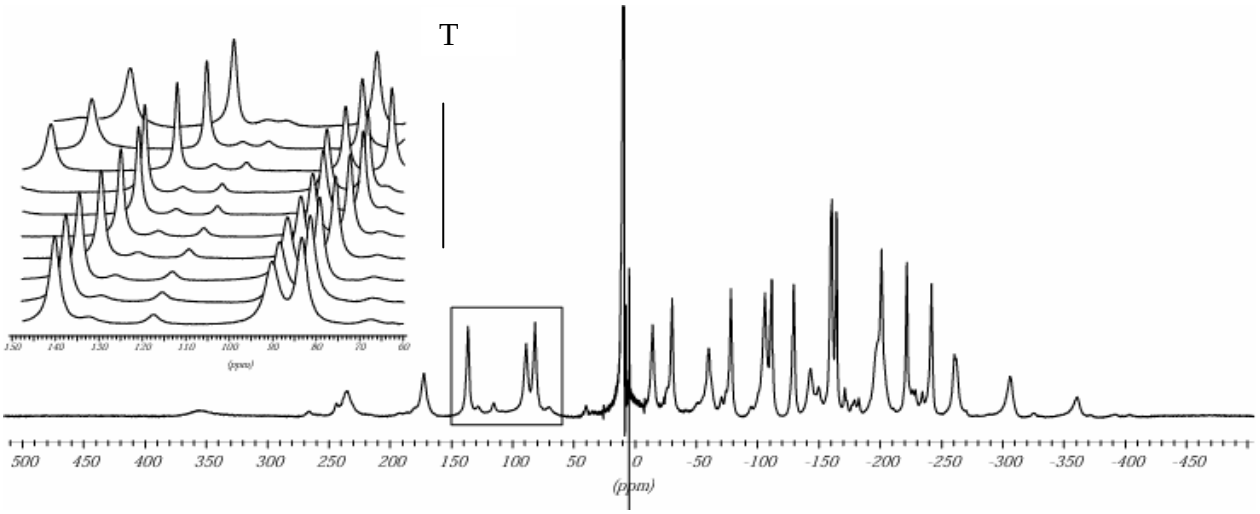

Figure S8. Temperature dependence of 400 MHz ^{1}H NMR spectra of $Tb_2(OHEC)^{2-}$.

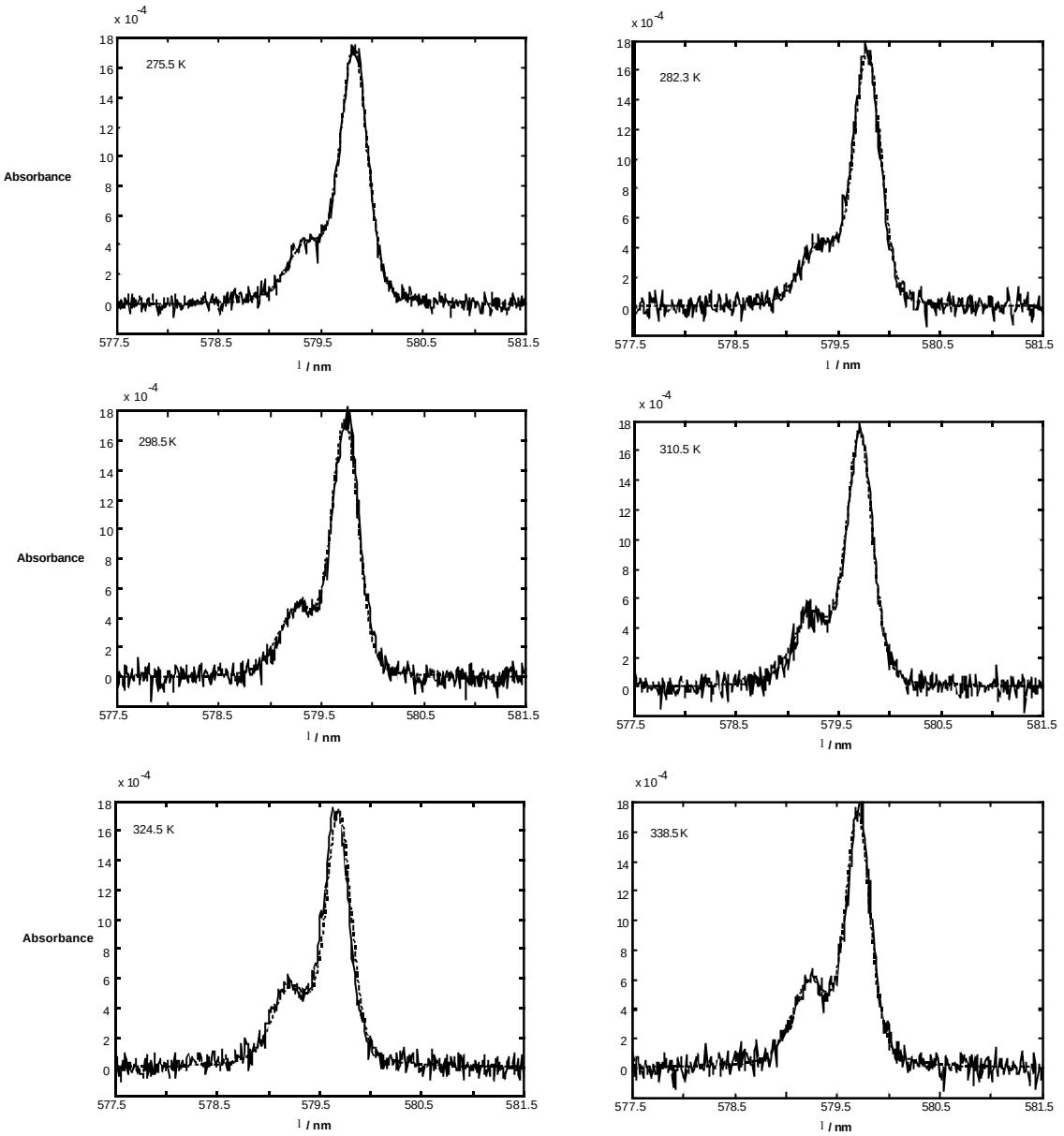

Figure S9. one dimensional representation of the temperature dependence of the $^7F_0$-$^5D_0$ transition on the UV-vis spectra of $Eu_2(OHEC)^{2-}$. C_{Eu} ~ 30 mmol kg^{-1}.

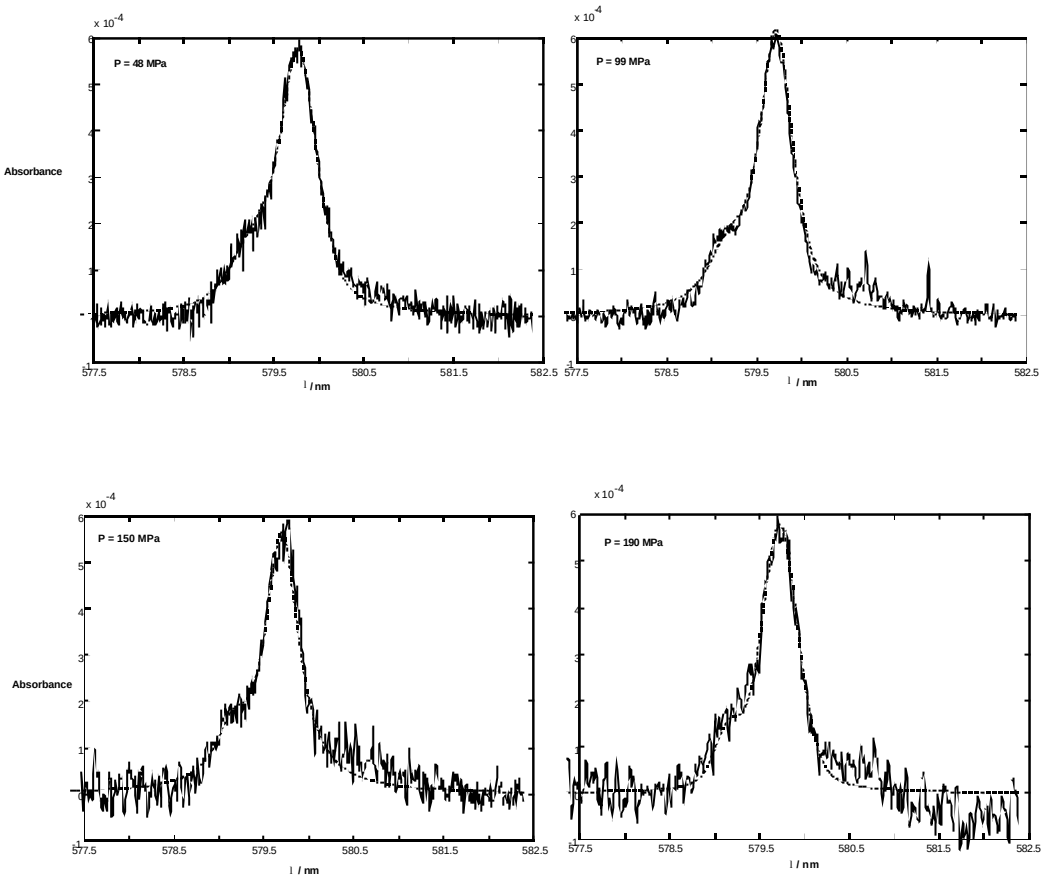

Figure S10. one dimensional representation of the pressure dependence of the $^7F_0$-$^5D_0$ transition at 298.2 K on the UV-vis spectra of $Eu_2(OHEC)^{2-}$. C_{Eu} ~ 10 mmol kg^{-1}.

Equations S1. The EPR spectra (S) are the sum of two spectra of each isomers weighted by their molar fraction x_α and x_β.

Each spectrum versus the magnetic field B can be then described as the sum of two derivatives one for the absorption part of the EPR spectrum (y_{ab}) and the other for the dispersion part (y_d). An additional term has then to be added for the baseline correction (described as linear versus the magnetic field).

The fitted parameters was done simultaneously for the 7 spectra with this following parameters, which were different for each spectrum except for the K^{298} and ΔH^0, which describe the equilibrium constant $K = X_\beta / X_\alpha$ (X_α and X_β are the molar fractions of the isomers α and β.): -Peak to peak line widths of the isomers α and β : $\Delta H_{pp,\alpha}$;$\Delta H_{pp,\beta}$

-Centre fields for the isomers α and β: $B_{0,\alpha}$; $B_{0,\beta}$

-the equilibrium constant, K (K^{298}, ΔH^0) extracted from the molar fractions of the isomers α and β (x_α; x_β) as $K = x_\beta / x_\alpha$.

-Phasing parameters for the absorption part : ϕ_1

-Phasing parameters for the dispersion part: ϕ_2

-Slope to describe the baseline: $basl_1$

-Origine ordinate to describe the baseline: $basl_2$

$$y_{ab}(\mathrm{i}) = \frac{\Delta H_{pp,i} \times \sqrt{3} \times (B_{0,i} - B)}{\left\{ \left(\frac{\Delta H_{pp,i} \times \sqrt{3}}{2} \right)^2 + (B_{0,i} - B)^2 \right\}^2} \qquad \text{Eq.S1}$$

$$y_d(\mathrm{i}) = \frac{(B_{0,i} - B)^2 - \left(\frac{\Delta H_{pp,i} \times \sqrt{3}}{2} \right)^2}{\left\{ \left(\frac{\Delta H_{pp,i} \times \sqrt{3}}{2} \right)^2 + (B_{0,i} - B)^2 \right\}^2} \qquad \text{Eq.S2}$$

For the global spectrum we obtained:

$$S = X_\alpha \times [\phi_1 \times y_{ab}(a) + \phi_2 \times y_d(a) + basl_1 \times B + basl_2] + X_\beta \times [\phi_1 \times y_{ab}(b) + \phi_2 \times y_d(b) + basl_1 \times B + basl_2] \qquad \text{Eq.S3}$$

Equations S2. The UV-vis spectra (S) are the sum of two spectra of each isomers weighted by their concentration C_α and C_β.

Each band can be described by a convolution gaussian-lorentzian. For a species i the following fitted parameters were different for each temperature except K^{298} and ΔH^0 and are:
-the area of the band, A_i
-the half line width of the band of i: Wi
-the centre of the band of i : C_i
-the ratio Gaussian compared to Lorentzian: Q
-the equilibrium constant, K (K^{298}, ΔH^0) extracted from the area of the bands of α and β x_β) as $K = A_\beta / A_\alpha$

For the band of i we obtained:

$$S_i = -2.77258872 \times \left(A_i - \frac{Q}{1+Q} A_i \right) \times \frac{W_i}{4 \times (X - C_i) + W_i^2} + 0.93943278 \left(\frac{Q}{1+Q} \frac{A_i}{W_i} \right) \times \exp\left\{ -2.77258872 \times (X - C_i)^2 \right\} \quad \text{Eq.S4}$$

For the global spectrum, S,we obtained:

$$S = S_\alpha + S_\beta \quad \text{Eq.S5}$$

The half line width and the centres of the band were assumed to have a linear dependence versus temperature and pressure.

Equations S3. From the measured ^{17}O NMR relaxation rates and angular frequencies of the paramagnetic solutions, $1/T_1$, $1/T_2$ and ω, and of the acidified water reference, $1/T_{1A}$, $1/T_{2A}$ and ω_A, the increase of the longitudinale and transverse relaxation rates, $1/T_1 - 1/T_{1A}$ and $1/T_2 - 1/T_{2A}$ respectively, and the decrease of the chemical shift, $\omega - \omega_A$ can be deduced (Eq.S6-8), where $1/T_{1m}$, $1/T_{2m}$ are the relaxation rates of the bound water and $\Delta\omega_m$ is the chemical shift difference between bound and bulk water, τ_m is the mean residence time or the inverse of the water exchange rate k_{ex} and P_m is the mole fraction of the bound water.[Swift, T.J.; Connick R.E. *J. Chem. Phys.* **1962**, *37*, 307.; Zimmermann, J. R.; Brittin, W. E. *J. Phys. Chem.* **1957,** *61*, 1328.] with $P_m = C_{Gd}/(1+K)$.

$$\left[\frac{1}{T_1}-\frac{1}{T_{1A}}\right]=P_m\left[\frac{1}{T_{1m}+t_m}+\frac{1}{T_{1os}}\right] \qquad \textbf{Eq.S6}$$

$$\left[\frac{1}{T_2}-\frac{1}{T_{2A}}\right]=P_m\left[\frac{1}{t_m}\frac{T_{2m}^{-2}+t_m^{-1}T_{2m}^{-1}+\Delta w_m^2}{(t_m^{-1}+T_{2m}^{-1})^2+\Delta w_m^2}+\frac{1}{T_{2os}}\right] \qquad \textbf{Eq.S7}$$

$$(w-w_A)=P_m\left[\frac{\Delta w_m}{(1+t_m T_{2m}^{-1})^2+t_m^2\Delta w_m^2}+\Delta w_{os}\right] \qquad \textbf{Eq.S8}$$

Previous studies have shown that outer sphere contributions to the ^{17}O relaxation rates, $1/T_{1os}$ and $1/T_{2os}$, are negligible [Micskei, K.; Helm, L.; Brücher, E.; Merbach, A. E. *Inorg. Chem.* **1993**, *32*, 3844] therefore no outer sphere contribution has been further considered.

The ^{17}O longitudinal relaxation rates in Gd^{III} solutions are the sum of the contributions of the dipole-dipole and quadrupolar (in the approximation developed by Halle) mechanisms as expressed by Eq.S9-11 for extreme narrowing conditions, where γ_S and γ_I are the electron and the nuclear gyromagnetic ratio respectively ($\gamma_S = 1.76\times10^{11}$ rad s^{-1} T^{-1}, $\gamma_I = -3.626\times10^7$ rad s^{-1} T^{-1}), r_{GdO} is the effective distance between the electron charge and the ^{17}O nucleus, I is the nuclear spin (5/2 for ^{17}O), χ is the quadrupolar coupling constant and η is an asymmetry parameter :

$$\frac{1}{T_{1m}} = \frac{1}{T_{1dd}} + \frac{1}{T_{1q}} \qquad \textbf{Eq.S9}$$

with:

$$\frac{1}{T_{1dd}} = \frac{2}{15}\left(\frac{\mu_0}{4\pi}\right)^2 \frac{\hbar^2 \gamma_I^2 \gamma_S^2}{r_{GdO}^6} S(S+1) \times \left[3J(\omega_I;\tau_{d1}) + 7J(\omega_S;\tau_{d2})\right] \qquad \textbf{Eq.S10}$$

$$\frac{1}{T_{1q}} = \frac{3p^2}{10}\frac{2I+3}{I^2(2I-1)} c^2 \times t_R \qquad \textbf{Eq.S11}$$

The spectral density function is expressed as in Eq S12.

$$J(\omega;\tau) = \left(\frac{\tau}{1+\omega^2\tau^2}\right) \qquad \textbf{Eq.S12}$$

The transverse relaxation of ^{17}O bound directly to Gd^{III} is governed by scalar relaxation and can be expressed by Eq.S13 with $\tau_{Si} = 1/\tau_m + 1/T_{ie}$ and where $\frac{A}{\hbar}$ is the scalar coupling constant.

$$\frac{1}{T_{2M}} = \frac{S(S+1)}{3}\left(\frac{A}{\hbar}\right)^2 \left(t_{S1} + \frac{t_{S2}}{1 + w_S^2 t_{S2}^2}\right) \qquad \textbf{Eq.S13}$$

The electronic longitudinal and transverse relaxation rate, $1/T_{1e}$ and $1/T_{2e}$, are principally dominated by the modulation of the zero field splitting for Gd^{III} chelates and are expressed in the following Eq.S14-15 , where Δ^2 is the mean square zero field splitting energy and τ_v is the correlation time for modulation of the zero field splitting interaction. This latter can be expressed by a simple Arrhenius law as written in eq S16, with t_v^{298} being the value of τ_v at 298.15 K and E_v the associated activation energy.

$$\frac{1}{T_{1e}} = \left(\frac{1}{T_{1e}}\right)^{ZFS} = \frac{1}{25}\Delta^2 t_v \left(4S(S+1) - 3\right)\left[\frac{1}{1 + w_S^2 t_v^2} + \frac{4}{1 + 4w_S^2 t_v^2}\right] \qquad \textbf{Eq.S14}$$

$$\frac{1}{T_{2e}} = \left(\frac{1}{T_{2e}}\right)^{ZFS} = \Delta^2 t_v \left[\frac{5.26}{1 + 0.372 w_S^2 t_v^2} + \frac{7.18}{1 + 1.24 w_S t_v}\right] \qquad \textbf{Eq.S15}$$

$$t_v = t_v^{298} \exp\left\{\frac{E_v}{R}\left(\frac{1}{T} - \frac{1}{298}\right)\right\}$$ **Eq.S16**

The transverse electronic relaxation rates, $1/T_{2e}$, for both homobinuclear and mixed Gd^{III}/Y^{III} complexes were directly calculated from the measured peak-to-peak EPR line widths, ΔH_{pp}, according to Eq. S17, where μ_B is the Bohr magneton and *h* the Planck constant.[J. Reuben *J. Chem. Phys.* **1971**, *75*, 3164]

$$\frac{1}{T_{2e}} = \frac{g_L \mu_B \pi \sqrt{3}}{h} \Delta H_{pp}$$ **Eq.S17**

The exchange rate is supposed to assume the Eyring equation. In eq S18 $\Delta S^{\ddagger}$ and $\Delta H^{\ddagger}$ are the entropy and enthalpy of activation for the water exchange process, and k_{ex}^{298} is the exchange rate at 298.15 K.

$$\frac{1}{\tau_m} = k_{ex} = \frac{k_B T}{h} exp\left\{\frac{\Delta S^{\ddagger}}{R} - \frac{\Delta H^{\ddagger}}{RT}\right\} = \frac{k_{ex}^{298} T}{298.15} exp\left\{\frac{\Delta H^{\ddagger}}{R}\left(\frac{1}{298.15} - \frac{1}{T}\right)\right\}$$ **Eq.S18**

In Eq S8, the chemical shift of the bound water molecule, $\Delta\omega_m$, depends on the hyperfine interaction between the Gd^{III} electron spin and the ^{17}O nucleus and is directly proportional to the scalar coupling constant, $\frac{A}{\hbar}$, as expressed in Eq.S19.[H.G. Brittain, J.F. Desreux *Inorg. Chem.* **1984**, *23*, 4459.]

$$\Delta\omega_m = \frac{g_L \mu_B S(S+1) B}{3 k_B T} \frac{A}{\hbar}$$ **Eq.S19**

The isotopic Landé g_L factor is equal to 2.0 for the Gd^{III}, B represents the magnetic field, and k_B is the Boltzmann constant.

The outer sphere term of the chemical shift was found proportional to $\Delta\omega_m$, through an empirical constant C_{os}.[G. Gonzalez, H.D. Powell, V.Tissières, A.E. Merbach *J. Phys. Chem.* **1994**, *98*, 53.]

$$\Delta\omega_{os} = C_{os}\Delta\omega_m \qquad \textbf{Eq.S20}$$

The measured longitudinal proton relaxation rate, R_1^{obs}, is the sum of a paramagnetic and a diamagnetic contribution as expressed in Eq S21, where r_1 is the proton relaxivity:

$$R_1^{obs} = R_1^d + R_1^p = R_1^d + r_1\,[Gd^{3+}] \qquad \textbf{Eq.S21}$$

The relaxivity can be divided into an inner and an outer sphere term as follows:

$$r_1 = r_{1is} + r_{1os} \qquad \textbf{Eq.S22}$$

Taking into account the contribution of each isomer to the relaxivity, r_1^a and r_1^b, weighted by their molar fraction we obtained:

$$r_1 = x_a\left(r_{1\mathrm{is}}^a + r_{1\mathrm{os}}^a\right) + x_b r_{1\mathrm{os}}^b \qquad \textbf{Eq.S23}$$

with x_a = (1/1+K) and x_b = 1- x_a with

$$r_{1is} = \frac{1}{1000}\times\frac{q}{55.55}\times\frac{1}{T_{1m}^H + \tau_m} \qquad \textbf{Eq.S24}$$

The longitudinal relaxation rate of the inner sphere protons, $1/T_{1m}{}^H$ is expressed by Eq S25, where r_{GdH} is the effective distance between the electron charge and the ^{1}H nucleus and was fixed to the common value of 3.1 angström, ω_I is the proton resonance frequency and ω_S is the Larmor frequency of the Gd^{III} electron spin.

$$\frac{1}{T_{1m}^H} = \frac{2}{15}\left(\frac{\mu_0}{4\pi}\right)^2 \frac{\hbar^2\gamma_I^2\gamma_S^2}{r_{GdH}^6} S(S+1)\times\left[3J\left(\omega_I;\tau_{d1}\right) + 7J\left(\omega_S;\tau_{d2}\right)\right] \qquad \textbf{Eq.S25}$$

$$\frac{1}{t_{di}} = \frac{1}{t_m} + \frac{1}{t_{RH}} + \frac{1}{T_{ie}} \qquad \textbf{Eq.S26}$$

With $\tau_{RH} = R_{OH} \times \tau_R$, where R_{OH} is the ratio of the rotational correlation times influencing the ^{17}O relaxation and the proton relaxation, respectively. The same activation energy was considered for the temperature dependence of both rotation correlation times.

The spectral density functions are given by Eq S12. The outer sphere contribution can be described by Eq.S27 where N_A is the Avogadro constant, and J_{os} is its associated spectral density function.[J. H. Freed *J. Chem. Phys.* **1978**, *68*, 4034; S.H. Koenig, RD. Brown III, *Prog. Nucl. Magn. Reson. Spectrosc.* **1991**, *22*, 487].

$$r_{1os}^{a,b} = \frac{32 N_A p}{405}\left(\frac{m_0}{4p}\right)^2 \frac{\hbar^2 g_S^2 g_I^2}{a_{GdH} D_{GdH}} S(S+1)\left[3J_{os}(w_I, T_{1e}^{a,b}) + 7J_{os}(w_S, T_{2e}^{a,b})\right] \qquad \textbf{Eq.S27}$$

$$J_{os}(\omega, T_{je}) = Re\left[\frac{1 + \frac{1}{4}\left(i\omega\tau_{GdH} + \frac{\tau_{GdH}}{T_{je}}\right)^{1/2}}{1 + \left(i\omega\tau_{GdH} + \frac{\tau_{GdH}}{T_{je}}\right)^{1/2} + \frac{4}{9}\left(i\omega\tau_{GdH} + \frac{\tau_{GdH}}{T_{je}}\right) + \frac{1}{9}\left(i\omega\tau_{GdH} + \frac{\tau_{GdH}}{T_{je}}\right)^{3/2}}\right] \qquad \textbf{Eq.S28}$$

j = 1, 2

The diffusion coefficient for the diffusion of a water proton away from a Gd^{III} complex, D_{GdH}, is assumed to obey an exponential law versus the inverse of the temperature, with an activation energy $E_{GdH,}$ as given in Eq.S29. D_{GdH}^{298} is the diffusion coefficient at 298.15K.

$$D_{GdH} = D_{GdH}^{298}\, exp\left\{\frac{E_{GdH}}{R}\left(\frac{1}{T} - \frac{1}{298.15}\right)\right\} \qquad \textbf{Eq.S29}$$

The correlation time, t_{GdH}, characteristic for the diffusion of a water proton away from the vicinity of the Gd^{III} is equal to $\frac{a_{GdH}^2}{D_{GdH}}$, with a_{GdH} the closest approach distance for a second sphere water proton to the Gd^{III} center fixed to 4.5 angström for the fit.

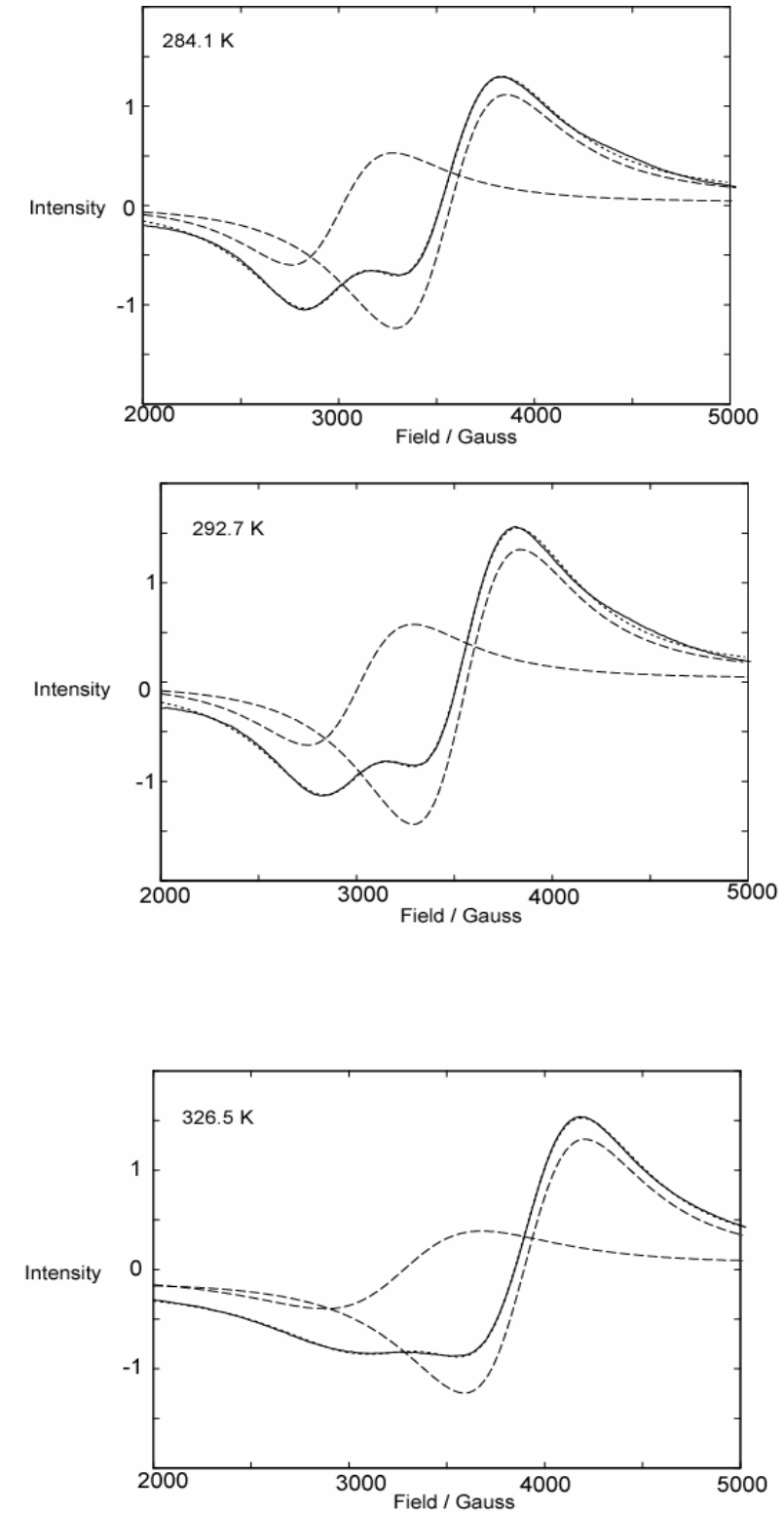

Figure S11. Temperature dependence of EPR spectra of the $Gd_2(OHEC)^{2-}$ and its *a* and *b* isomers at X-band. The dotted lines represent the calculated spectra calculated for each isomer.

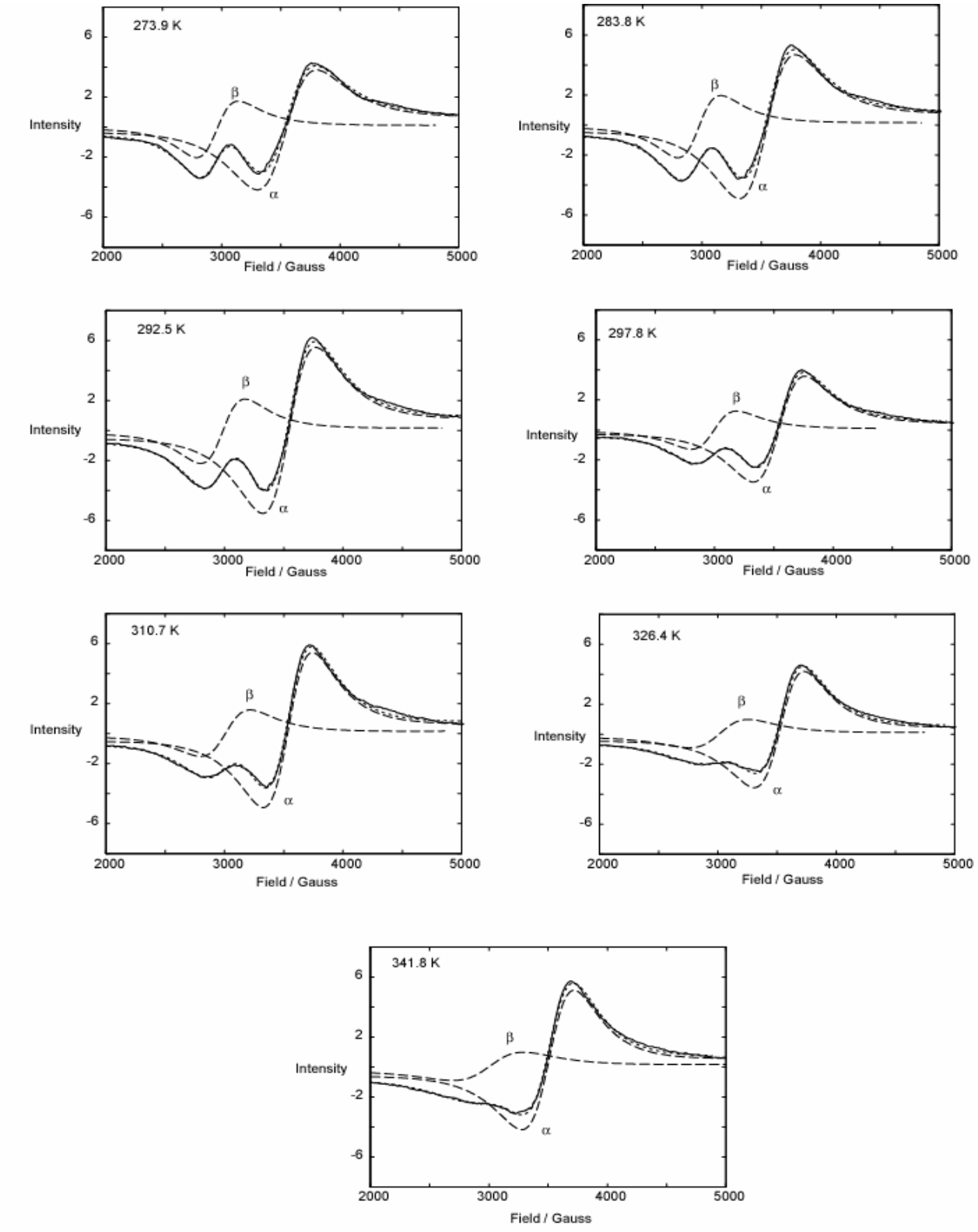

Figure S12. Temperature dependence of EPR spectra of the $GdY(OHEC)^{2-}$ and its *a* and *b* isomers at X-band. The dotted lines represent the calculated spectra calculated for each isomer.

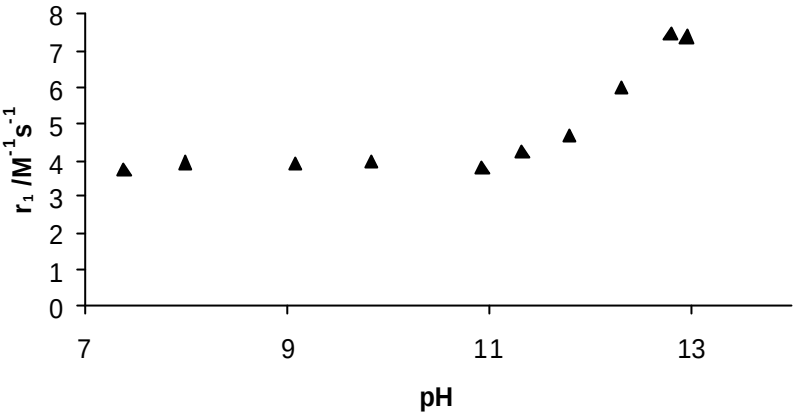

Figure S13. pH dependence of the relaxivity of $Gd_2(OHEC)^{2-}$ at 298.2 K.

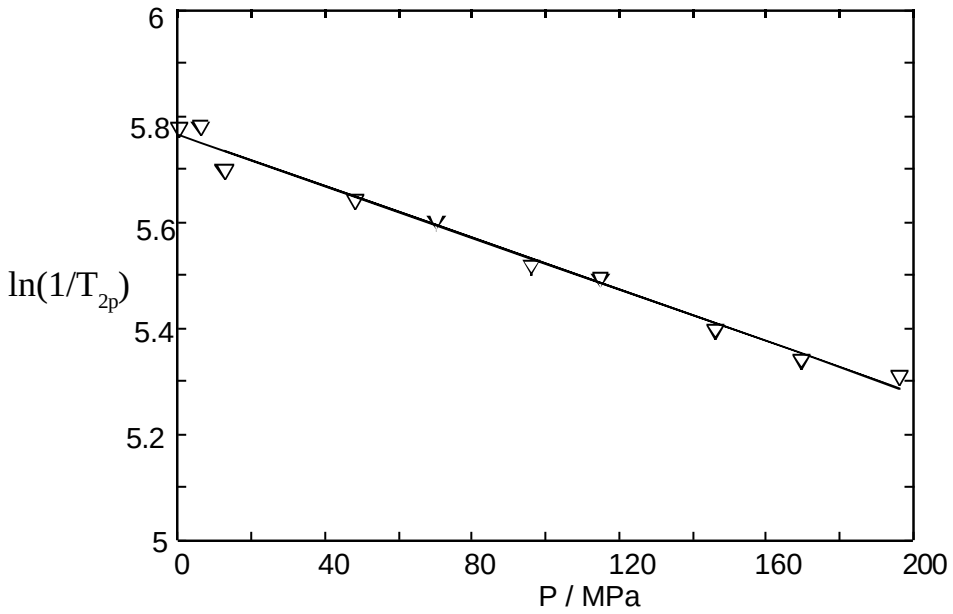

Figure S14. Pressure dependence of the increase of the ^{17}O transverse relaxation rate ($1/T_{2p}$) at 312 K and 9.4 T due to $[Gd_2(OHEC)(H_2O)_2]^{2-}$. C_{Gd} = 45.17 mmol kg^{-1}

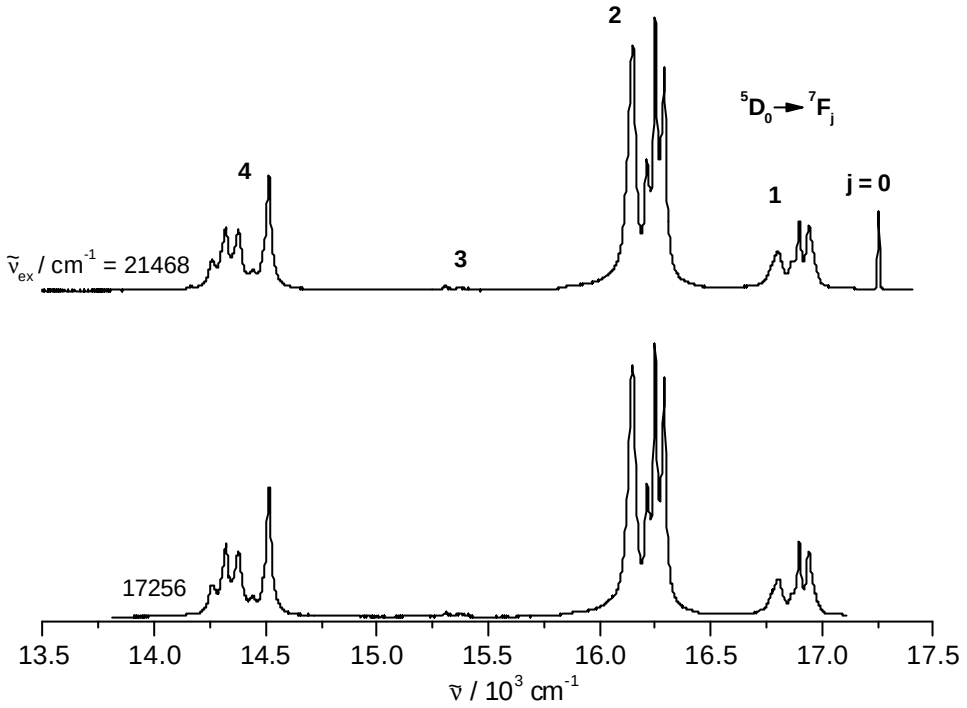

Figure S15. Emission spectra of the $Na_2[Eu_2.OHEC.(H_2O)_2]$ complex in solid state at 295 K, upon broad ($^5D_2$) band and selective excitation.

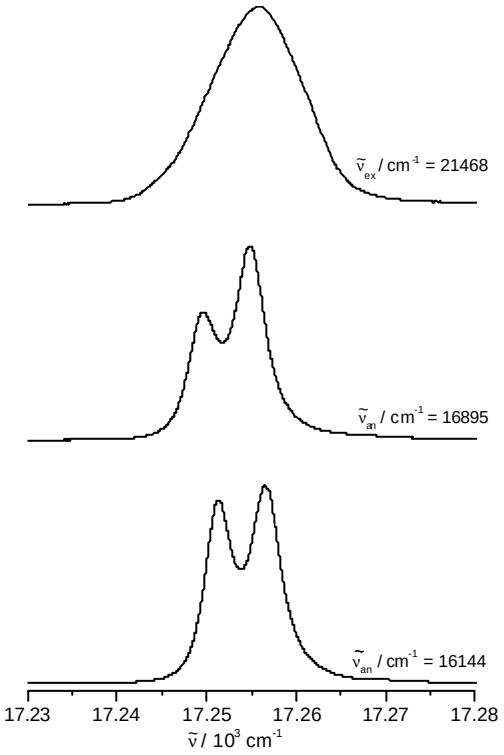

Figure S16. Excitation spectra at 295 K of the $Na_2[Eu_2.OHEC.(H_2O)_2]$ complex in solid state, upon monitoring the Eu($^5D_0 \rightarrow {}^7F_{1,2}$) transitions and enlargement (top) of the Eu($^5D_0 \rightarrow {}^7F_0$) transition (broad band excitation($^5D_2$)).

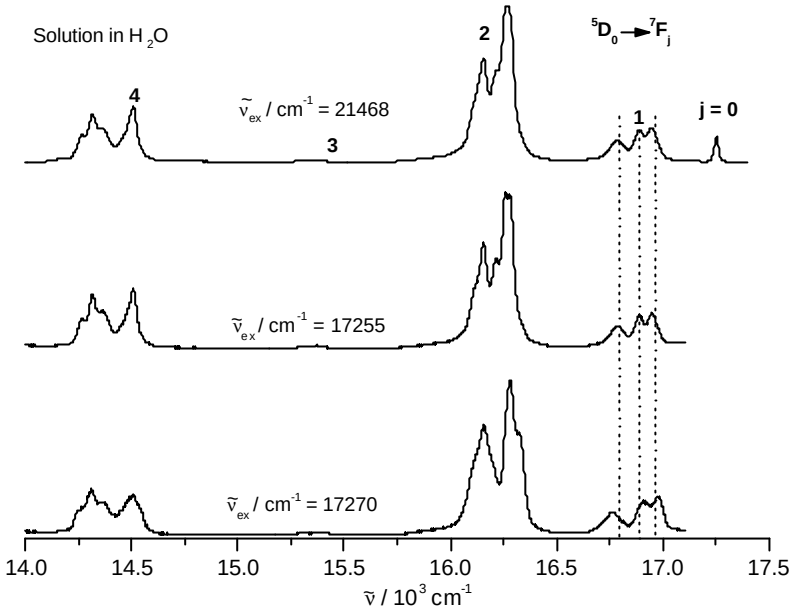

Figure S17. Emission spectra of the $[Eu_2(OHEC)]^{2-}$ complex in solution (10^{-3} M), at 295 K, upon broad band ($^5D_2$) and selective excitation.

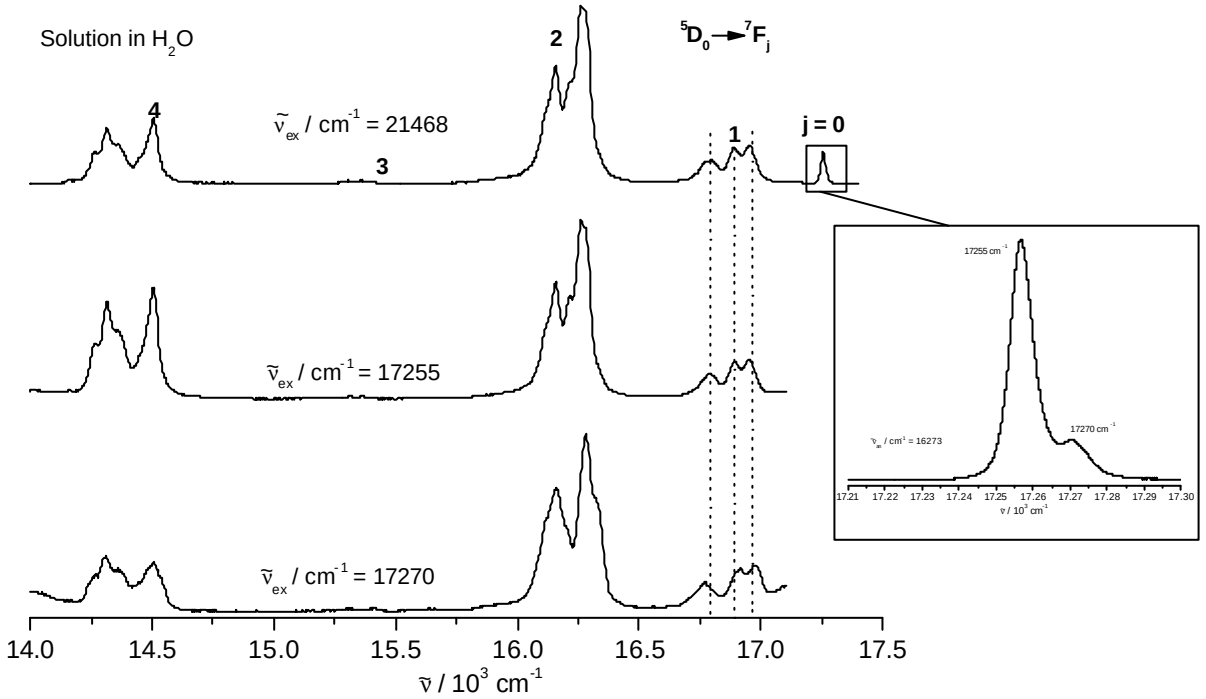

Figure S18. Emission spectra of the $[Eu_2(OHEC)]^{2-}$ complex in solution (10^{-4} M), at 295 K, upon broad band and selective excitation.

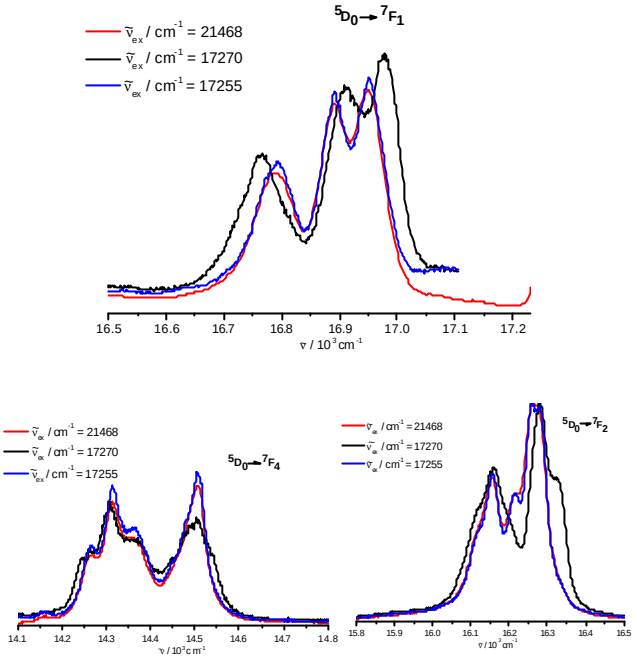

Figure S19. Normalised emission spectra of the $[Eu_2(OHEC)]^{2-}$ complex in solution (10^{-3} M), at 295 K, upon broad band and selective excitation.

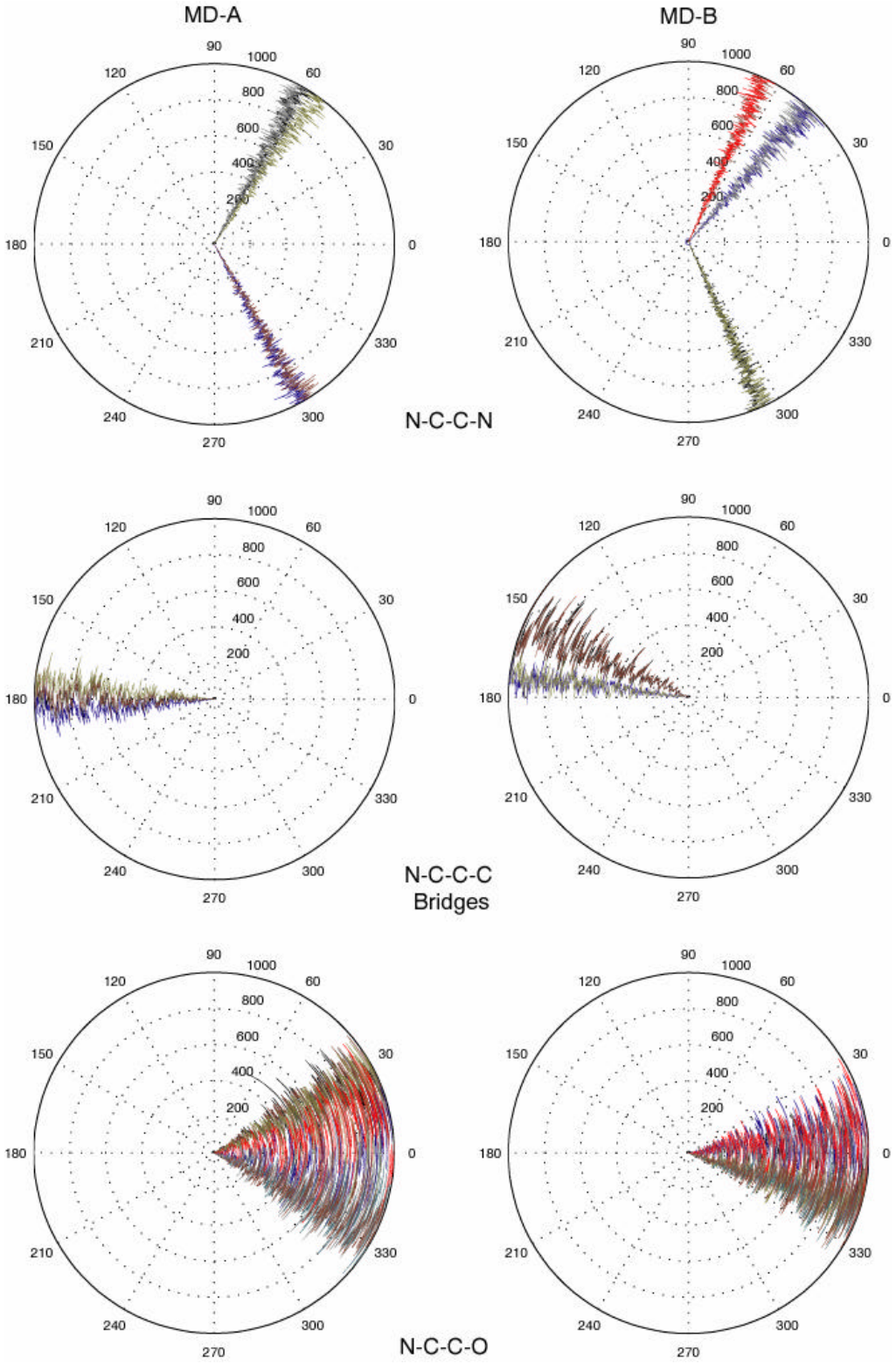

Figure S20. Time evolution of the α and β isomers dihedral angles during the simulations MD-*a* and MD-*b*. The radial part represent the time in picosecond while the azimutal angle angle represent the dihedral angles.

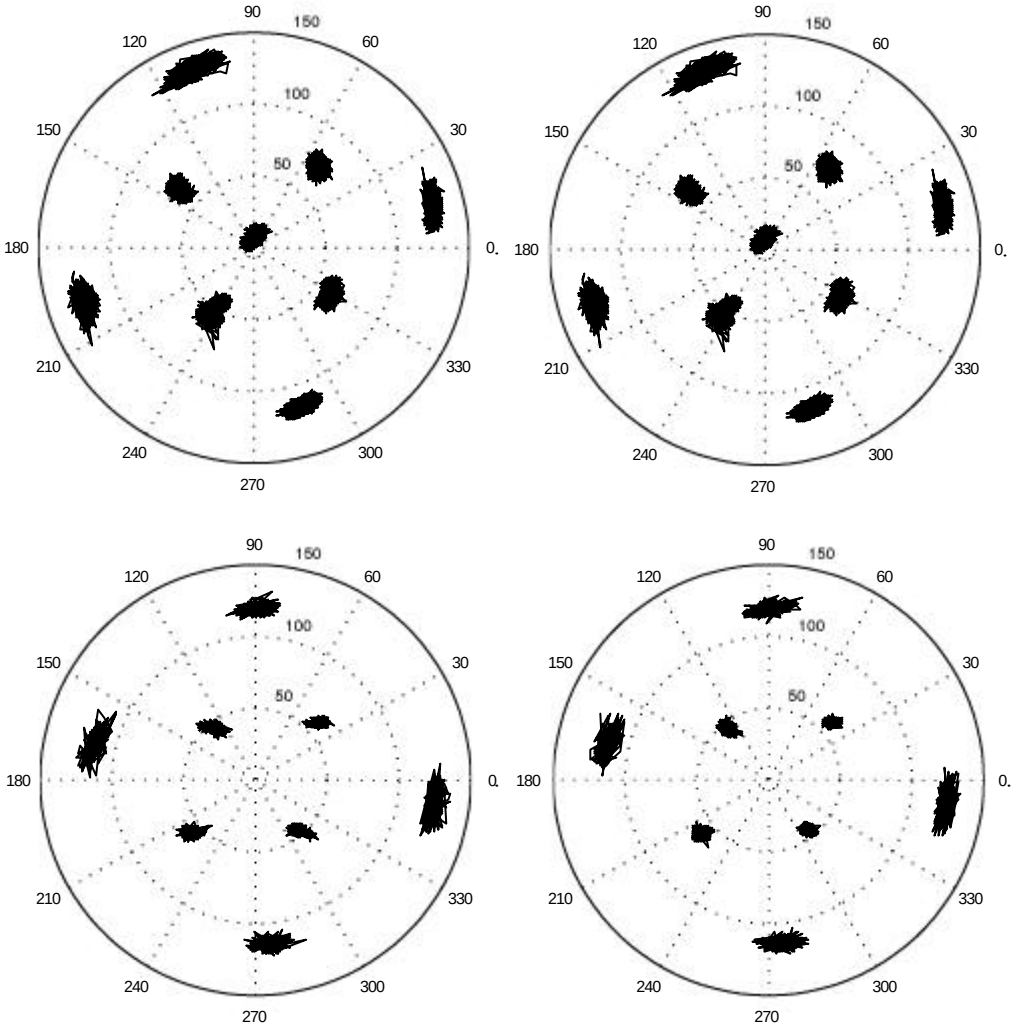

Figure S21. Angular projections of the Gd^{III} coordination polyhedrons centred on the C_4 axis. Upper part : projection of the two coordination polyhedrons in MD-a. Lower part : corresponding projections in MD-b.

Table S1. Ratio of the molar fraction of the 2 isomers *a* and *b* of $Eu_2(OHEC)^{2-}$, $x_b/x_a = K$, obtained from the 600MHz ^1H NMR study at variable temperature.

T / K	x_b/x_a	$\ln(x_b/x_a) = \ln(K)$
273.7	0.36	-1.03
279.5	0.38	-0.96
284.6	0.39	-0.94
289.7	0.42	-0.87
294.9	0.43	-0.85

Table S2. Ratio of the molar fraction of the 2 isomers *a* and *b* of $Eu_2(OHEC)^{2-}$, $x_b/x_a = K$, obtained from the variable pressure study at 400 MHz and, at 279.4 K

P	$\ln(K)$
0	-1.01
14	-1.00
58	-1.06
82	-1.10
108	-1.15
125	-1.15
147.5	-1.20
184	-1.25

Table S3. Half line widths ($1/T_2$) of the protons ^{2}E', ^{2}e' (×2) from the experimental 600 MHz ^{1}H NMR spectra of $Eu_2(OHEC)^{2-}$ measured at variable temperature.

T / K	$1/T_{2,\ 2E'}$ / Hz	$1/T_{2,\ 2e'}$ / Hz	$1/T_{2,\ 2e'}$ / Hz
274.8	104.8	128.48	128.4
278.9	102.7	128.86	138.5
283.8	102.0	128.92	153.6
288.9	108.3	133.77	187.7
293.8	122.4	144.83	250.2
298.9	148.6	168.17	384.3

Table S4. Extrapolated half line widths ($1/T_2$) of the protons ^{2}E', ^{2}e' (×2) from the experimental 600 MHz ^{1}H NMR spectra of $Eu_2(OHEC)^{2-}$ measured at variable temperature.

T / K	$1/T_{2,\ 2E'}$ / Hz	$1/T_{2,\ 2e'}$ / Hz	$1/T_{2,\ 2e'}$ / Hz
274.8	98.1	106.0	108.4
278.9	91.2	114.5	107.7
283.8	83.8	125.1	106.9
288.9	76.9	136.7	106.0
293.8	71.1	148.5	105.3
298.9	65.6	161.4	104.5
309.8	55.9	191.0	102.9
319.5	48.8	219.8	101.7

Table S5. Isomerisation constant, k_{is}, obtained from the simulation of the experimental 600 MHz ^{1}H NMR spectra of $Eu_2(OHEC)^{2-}$ measured at variable temperature with the formalism of Kubo-Sack and a 3 sites exchange matrix (protons: ^{2}E', ^{2}e' (×2)) .

T / K	k_{is} / s^{-1}
274.8	6.8
278.9	12.6
283.8	16.7
288.9	30.2
293.8	51.3
298.9	83.1
309.8	219.8
319.5	582

Table S6. Half line widths ($1/T_2$) of the protons ^{2}E', ^{2}e' (×2) from the experimental 400 MHz ^{1}H NMR spectra of $Eu_2(OHEC)^{2-}$ measured at variable pressure and at 279.4 K.

T / K	$1/T_{2,\ 2E'}$ / Hz	$1/T_{2,\ 2e'}$ / Hz	$1/T_{2,\ 2e'}$ / Hz
0	127.2	163.8	158.3
14	127.9	162.8	151.7
58	130.0	159.8	133.0
82	148.1	138.8	128.0
108	140.7	121.5	120.6

Table S7. Extrapolated half line widths of the experimental 400 MHz ^{1}H NMR spectra of $Eu_2(OHEC)^{2-}$ measured at variable pressure and at 279.4 K.

P / Mpa	$1/T_{2,\ 2E'}$ / Hz	$1/T_{2,\ 2e'}$ / Hz	$1/T_{2,\ 2e'}$ / Hz
0	113.7	132.2	120.0
14	115.5	127.8	116.0
58	121.2	115.0	104.4
82	124.5	108.6	98.6
108	128.1	102.0	92.6
125	130.5	97.9	88.9
147.5	133.8	92.8	84.2
184	139.3	85.0	77.2

Table S8. Kinetics constant, k_{is} ($a \underset{}{\overset{k_{is}}{\rightleftarrows}} b$), obtained from the simulation of the experimental 400 MHz ^{1}H NMR spectra of $Eu_2(OHEC)^{2-}$ measured at variable pressure with the formalism of Kubo-Sack and a 3 sites exchange matrix (protons: ^{2}E', ^{2}e' (×2)) .

P / MPa	k_{is} / s^{-1}
0	14.5
14	13.8
58	12.0
82	10.0
108	10.8
125	9.4
147.5	8.7
184	7.7

Table S9. ^{17}O observed longitudinal and transverse relaxation rates at 9.4 T as a function of temperature for the diamagnetic reference at pH = 9.0 ($1/T_{1A}$ and $1/T_{2A}$) and in the presence of $Gd_2(OHEC)^{2-}$ ($1/T_1$ and $1/T_2$). Solution of $Gd_2(OHEC)^{2-}$: C_{Gd} = 21.87 mmol kg^{-1}.

T / K	$1/T_{1A}$ / s-1	$1/T_{2A}$ / s-1	$1/T_1$ / s-1	$1/T_2$ / s-1	$\ln(1/T_1-1/T_{1A})$	$\ln(1/T_2-1/T_{2A})$
270.5	353.9	376.3	364.0	-	2.32	-
277.2	270.3	289.2	281.4	337.7	2.40	3.88
284.7	210.0	223.8	219.3	281.1	2.23	4.05
292.4	163.7	176.8	174.3	275.0	2.37	4.59
295.2	151.1	163.2	160.8	270.4	2.27	4.68
302.1	125.8	137.0	134.8	267.1	2.20	4.87
308.2	107.9	118.5	115.5	270.0	2.02	5.02
311.7	101.1	109.2	108.0	275.3	1.93	5.11
318.6	87.7	96.7	94.1	288.6	1.85	5.26
325.6	75.8	83.7	80.9	308.3	1.62	5.41
335.6	63.2	72.9	67.7	340.2	1.49	5.59

Table S10. ^{17}O chemical shift of the diamagnetic reference, δ_A, and in the presence of $Gd_2(OHEC)^{2-}$ at pH = 9.0, δ, at 9.4 T as a function of temperature. Solution of $Gd_2(OHEC)^{2-}$: C_{Gd} = 21.87 mmol kg^{-1}.

T / K	δ_A / Hz	δ / Hz	$\omega-\omega_A$ / rad s^{-1}
281.1	-3494	-3501	-43.96
290.7	-3514	-3519	-31.40
300.9	-3542	-3549	-43.96
310.4	-3560	-3560.3	-1.88
320.4	-3579	-3584	-31.40
329.1	-3604	-3608.2	-26.38
339.2	-3631.3	-3634.6	-20.72

Table S11. Pressure dependence of the increase of the ^{17}O transverse relaxation rate ($1/T_{2P} = 1/T_{2,obs} - 1/T_{2A}$) due to $[Gd_2(OHEC)(H_2O)_2]^{2-}$ at pH = 9.0 and of the diamagnetic reference ($1/T_{2A}$) (bidistilled water at pH =9.0) at 312 K and 9.4 T. C_{Gd} = 45.17 mmol kg^{-1}

P / MPa	$1/T_{2,obs}$ / s^{-1}	$1/T_{2A}$/ s^{-1}	$\ln(1/T_{2p})$
0.2	428.33	105.48	5.78
6.1	429.09	105.13	5.78
48.4	384.39	102.63	5.64
96.3	349.37	99.80	5.52
146.1	317.57	96.86	5.40
196.5	296.12	93.88	5.31
169.5	304.06	95.47	5.34
115	341.93	98.69	5.49
70.3	372.65	101.34	5.60
12.6	403.23	104.75	5.70

Table S12. ^{17}O transverse relaxation rates at 4.7 T as a function of temperature for the diamagnetic reference at pH = 9 ($1/T_{2A}$) and in the presence of $Gd_2(OHEC)^{2-}$ ($1/T_2$). Solutions of $Gd_2(OHEC)^{2-}$: C_{Gd} = 21.87 mmol kg^{-1}.

T / K	$1/T_{2A}$ / s-1	$1/T_2$ / s-1	$\ln(1/T_2 - 1/T_{2A})$
272.0	142.9	169.25	3.27
281.6	193.6	234.81	3.72
290.2	248.3	311.93	4.15
301.0	331.9	424.14	4.52
304.7	107.3	207.85	4.61
313.6	134.9	265.25	4.87
322.3	83.0	216.86	4.90
328.6	82.0	227.43	4.98
337.5	50.2	235.87	5.22

Table S13. Half line widths (W) and centres (C) of the bands of α and β isomers measured at variable temperature by UV-vis. The obtained equilibrium constant *K* is given for each temperature. C_{Eu} ~ 30 mmol kg^{-1}.

T / K	W_α / cm^{-1}	W_β / cm^{-1}	C_α / cm^{-1}	C_β / cm^{-1}	$K^{a)}$
275.5	9.4	14.5	17247.2	17260.9	0.35
282.3	9.3	14.4	17247.7	17261.3	0.36
298.5	9.2	14.0	17248.7	17262.4	0.40
310.5	9.1	13.8	17249.5	17263.3	0.42
324.5	9.0	13.4	17250.4	17264.2	0.45
338.5	8.8	13.1	17251.3	17265.2	0.48

[a)] *K* values calculated from the fitted K^{298} and ΔH^0 values

Table S14. Half line widths (W) and centres (C) of the bands of α and β isomers measured at variable pressure by UV-vis. The obtained equilibrium constant *K* is given for each temperature. C_{Eu} ~ 10 mmol kg^{-1}.

P / MPa	W_α / cm^{-1}	W_β / cm^{-1}	C_α / cm^{-1}	C_β / cm^{-1}	$K^{a)}$
48	14.0	24.0	17250.1	17260.6	0.31
99	13.8	20.7	17252.0	17262.5	0.24
150	13.6	17.4	17254.0	17264.5	0.19
190	13.4	14.9	17255.5	17266.0	0.15

[a)] *K* values calculated from the fitted K^{298} and ΔH^0 values

Table S15. Peak to peak line widths and resonance frequency of the EPR spectra of $Gd_2(OHEC)^{2-}$, for its two *a* and *b* isomers, and the equilibrium constant *K*, as a function of temperature at the X-band (0.34 T). Solutions of $Gd_2(OHEC)^{2-}$: C_{Gd} = 40.7 mmol kg^{-1}.

T / K	$\Delta H_{pp,a}$ / Gauss	$\Delta H_{pp,b}$/ Gauss	$B_{0,a}$ / Gauss	$B_{0,b}$ / Gauss	$K^{a)}$
273.9	582.5	502.1	3541.3	2983.7	0.38
284.1	562.9	516.5	3542.5	2991.0	0.40
292.7	547.0	537.8	3542.1	2998.6	0.42
298.3	652.3	663.3	3917.9	3255.7	0.44
311.2	626.7	712.7	3913.3	3270.9	0.47
326.5	610.0	788.2	3903.6	3285.4	0.50
342.7	615.2	875.8	3890.7	3285.9	0.54

[a)] *K* values calculated from the fitted K^{298} and ΔH^0 values

Table S16. Water proton relaxivity, r_1 (in $mM^{-1}s^{-1}$) of $Gd_2(OHEC)^{2-}$ as a function of temperature and magnetic field. Solution of $Gd_2(OHEC)^{2-}$, C_{Gd} = 1.88 mmol dm^{-3}.

	r_1 / $mM^{-1}s^{-1}$				
^{1}H n / MHz	**5 °C**	**15 °C**	**25 °C**	**37°C**	**50 °C**
10.00	3.78	3.32	3.66	3.89	3.82
6.00	4.21	3.84	4.14	4.33	4.11
3.60	4.46	4.05	4.34	4.55	4.76
2.16	4.67	4.17	4.46	4.77	4.91
1.30	4.62	4.55	4.46	4.76	4.86
0.78	4.72	4.48	4.71	4.88	4.91
0.47	4.96	4.52	4.66	4.84	4.70
0.28	4.96	4.53	4.73	4.89	4.96
0.17	5.04	4.53	4.63	4.85	5.08
0.10	4.99	4.57	4.57	4.67	5.09
0.06	5.00	4.44	4.57	4.76	4.99
0.04	4.88	4.54	4.71	4.83	4.90
12.00	3.74	3.39	3.48	3.75	3.54
14.00	3.57	3.29	3.42	3.54	3.39
16.00	3.48	3.00	3.31		3.33
40.00	3.28	3.12	3.19	3.22	2.93
29.00	3.31	3.14	3.20	3.28	3.08
50.10	3.28	3.22	3.25	3.12	2.93
20.00	3.51	3.28	3.41	3.45	3.18
200.00	3.04	2.90	2.98	3.05	2.89

Table S17. Peak to peak line widths and resonance frequency of the EPR spectra of $GdY(OHEC)^{2-}$ for its two *a* and *b* isomers, and the equilibrium constant *K*, as a function of temperature at the X-band (0.34 T). Solutions of $GdY(OHEC)^{2-}$: C_{Gd} = 5.3 mmol kg^{-1}.

T / K	$\Delta H_{pp,a}$ / Gauss	$\Delta H_{pp,b}$/ Gauss	$B_{0,a}$ / Gauss	$B_{0,b}$ / Gauss	$K^{a)}$
273.9	494.2	349.7	3525.6	2945.8	0.24
283.8	467.0	360.4	3535.9	2965.7	0.26
292.5	444.6	372.7	3541.4	2981.6	0.27
297.8	431.2	381.3	3543.0	2994.1	0.28
310.7	412.0	415.0	3542.6	3014.8	0.30
326.4	415.4	486.1	3537.5	3031.9	0.33
341.8	434.3	580.6	3527.2	3033.4	0.36

[a)] *K* values calculated from the fitted K^{298} and ΔH^0 values

Table S18: Integrated and corrected relative intensities of the Eu($^5D_0 \rightarrow {}^7F_j$) transitions at 295 K.

	n_{ex}^2 / cm^{-1}	$\int_{0\rightarrow0}$	$\int_{0\rightarrow1}$	$\int_{0\rightarrow2}$	$\int_{0\rightarrow3}$	$\int_{0\rightarrow4}$
Solid state	21468	0.11	1.00	4.41	0.03	1.64
	17256	-	1.00	4.46	0.03	1.80
Solution in H_2O (10^{-3} M)	21468	0.09	1.00	4.24	0.04	1.56
	17255	-	1.00	4.90	0.04	2.05
	17270	-	1.00	4.31	0.05	1.57
Solution in D_2O (10^{-3} M)	21468	0.12	1.00	4.12	0.04	1.53
	17255	-	1.00	4.72	0.03	1.84
	17270	-	1.00	4.35	0.04	1.43

Table S19. Energy (cm^{-1}) of the identified crystal-field sub-levels of the Eu(^7F_j) manifold (J = 1-4) in $Eu_2(OHEC)^{2-}$ as determined from excitation and emission spectra in solid state or in water solution at 295 K; $^7F_0$ is taken as the origin.

	Solid state		Water solution				Solid state		Water solution		
n_{ex}^2 / cm^{-1}	21468	17256	21468	17270	17256		21468	17256	21468	17270	17256
site				I	II					I	II
$^5D_0$	17256	17256	17255	17270	17256	$^7F_3$	1845	1846	1852	1860	1840
							1866	1882	1887	1911	1882
$^7F_1$	315	314	303	296	296		1946	1945	1941	1973	1936
	358	357	361	362	358						
	390	389				$^7F_4$	2741	2740	2748	2772	2742
	453	451	462	510	454		2812	2812			
							2876	2878	2890	2913	2888
$^7F_2$	964	963	981	950	966		2934	2935	2937	2967	2936
	1005	1004		994	990		2995	2997	2980	3025	2982
	1041	1040	1036		1033		3091	3089	3087	3105	3090
	1105	1108	1094	1113	1092						

Table S20. Lifetimes of the Eu($^5D_0$) excited level (ms) in $Eu_2(OHEC)^{2-}$ under various excitation conditions (analysing wavelength set on the maximum of the $^5D_0 \rightarrow {}^7F_2$);2 σ is given within parentheses.

T / K Eu$_2$O-HEC	n^2_{ex} / cm^{-1}	n^2_{an} / cm^{-1}	t /ms	
Solution in H_2O				
	28170	16279	0.92(4)	0.53(5)
	17275	16793	0.98(2)	
	17270		1.01(2)	
	17255	17000	0.55(2)	
	17249		0.57(3)	
Solution in D_2O				
	28170	16279	1.68(7)	
	17275	16793	1.72(1)	
	17270		1.71(2)	
	17255	17000	1.65(2)	
	17249		1.62(2)	

Table S21. Calculated number of water molecules q.

n^2_{ex} / cm^{-1}	Solution in H_2O		Solution in D_2O	$q = 1.05(\Delta k_{obs})$		$q = 1.2(\Delta k_{obs} - 0.25)$		$q = 1.11(\Delta k_{obs} - 0.31)$	
	t /ms		t /ms						
28170 site β, α	0.92	0.53	1.68	0.5	1.4	0.3	1.2	0.2	1.1
17275 site β	0.98		1.72	0.5		0.2		0.1	
17270 site β	1.01		1.71	0.4		0.2		0.1	
17255 site α	0.55		1.65	1.3		1.2		1.0	
17249 site α	0.57		1.62	1.2		1.1		0.9	

Table S22. Selected time averaged dihedral angles calculated from MD simulations. Numbers in brackets are one standard deviation.

Angle / °	MD-α	conf.	MD-β	conf.
I	60 (6)	δ	-66 (6)	λ
II	-56 (6)	λ	48 (7)	δ
III	-62 (7)	λ	65 (6)	δ
IV	-60 (6)	λ	-66 (6)	λ
V	56 (6)	δ	49 (7)	δ
VI	61 (7)	δ	65 (6)	δ
VII	181 (8)	a	156 (11)	p
VIII	186 (8)	a	173 (8)	a
IX	180 (8)	a	156 (11)	p
X	174 (8)	a	173 (8)	a
XI	23 (17)	δ	5 (15)	δ
XII	-9 (18)	λ	7 (17)	δ
XIII	27 (14)	δ	-19 (13)	λ
XIV	22 (18)	δ	-16 (13)	λ
XV	-23 (16)	λ	7 (14)	δ
XVI	10 (19)	δ	7 (17)	δ
XVII	-25 (15)	λ	-19 (13)	λ
XVIII	-24 (17)	λ	-15 (13)	λ